RhoB controls endothelial barrier recovery by inhibiting Rac1 trafficking to the cell border

Beatriz Marcos-Ramiro,[1] Diego García-Weber,[1] Susana Barroso,[1] Jorge Feito,[2] María C. Ortega,[1] Eva Cernuda-Morollón,[3] Natalia Reglero-Real,[1] Laura Fernández-Martín,[1] Maria C. Durán,[4] Miguel A. Alonso,[1] Isabel Correas,[1] Susan Cox,[5] Anne J. Ridley,[5] and Jaime Millán[1]

[1]Centro de Biología Molecular Severo Ochoa, Consejo Superior de Investigaciones Cientificas, Universidad Autónoma de Madrid, 28049 Madrid, Spain
[2]Servicio de Anatomía Patológica, Hospital Universitario de Salamanca, 37007 Salamanca, Spain
[3]Neurology Department, Hospital Universitario Central de Asturias, 33011 Oviedo, Spain
[4]Biomedicine, Biotechnology and Public Health Department, University of Cadiz, 11519 Cadiz, Spain
[5]Randall Division of Cell and Molecular Biophysics, King's College London, SE1 1UL London, England, UK

Endothelial barrier dysfunction underlies chronic inflammatory diseases. In searching for new proteins essential to the human endothelial inflammatory response, we have found that the endosomal GTPase RhoB is up-regulated in response to inflammatory cytokines and expressed in the endothelium of some chronically inflamed tissues. We show that although RhoB and the related RhoA and RhoC play additive and redundant roles in various aspects of endothelial barrier function, RhoB specifically inhibits barrier restoration after acute cell contraction by preventing plasma membrane extension. During barrier restoration, RhoB trafficking is induced between vesicles containing RhoB nanoclusters and plasma membrane protrusions. The Rho GTPase Rac1 controls membrane spreading and stabilizes endothelial barriers. We show that RhoB colocalizes with Rac1 in endosomes and inhibits Rac1 activity and trafficking to the cell border during barrier recovery. Inhibition of endosomal trafficking impairs barrier reformation, whereas induction of Rac1 translocation to the plasma membrane accelerates it. Therefore, RhoB-specific regulation of Rac1 trafficking controls endothelial barrier integrity during inflammation.

Introduction

In response to infection, tissue damage, or chronic inflammation, cells produce proinflammatory cytokines such as TNF, interleukin-1β (IL-1β), andIFN-γ that have pleiotropic effects on blood vessels surrounding the inflammatory focus. These cytokines trigger a transcriptional program in the endothelium to express proteins necessary for a long-term inflammatory response, including those involved in altering endothelial barrier function. The pathological expression of some of these proteins contributes to the development of inflammatory and thrombotic diseases (Libby, 2002; Compston and Coles, 2008; Khan et al., 2010).

The family of Rho GTPases contains more than 20 members that regulate multiple cellular functions. The founder member of this family, RhoA, is closely related to RhoB and RhoC. These three GTPases are often considered as a RhoA subfamily whose members share 88% amino acid identity and have the potential to regulate common effectors, such as Rho kinases (ROCKs; Ridley, 2013). However, RhoA, RhoB, and RhoC have remarkably different effects on cancer cell migration, which indicate that they also regulate different signaling pathways (Ridley, 2013). The three GTPases in their active state are associated with the plasma membrane, but only RhoB is also localized to the endosomal compartment (Ridley, 2013). In the endothelium, the signaling pathways controlled by the RhoA subfamily are essential for maintaining the barrier integrity, mainly by regulating ROCKs, which drive actomyosin-mediated contractile force generation and modulate cell–cell junctions (Wojciak-Stothard and Ridley, 2002; van Nieuw Amerongen et al., 2007; Vandenbroucke et al., 2008). Despite the importance of this signaling pathway, the relative contribution of each RhoA subfamily member to endothelial barrier function has not been yet characterized. On the other hand, the plasma membrane localization of another Rho GTPase, Rac1, is central to endothelial cell–cell junction remodeling and stabilization (Garcia et al., 2001; Cain et al., 2010; Marcos-Ramiro et al., 2014). Interestingly, Rac1 endosomal internalization and recycling are necessary for the polarized targeting and function of this GTPase to plasma membrane domains, such as circular

Correspondence to Jaime Millán: jmillan@cbm.csic.es

Abbreviations used in this paper: DN, dominant negative; FA, focal adhesion; HDMVEC, human dermal microvascular endothelial cell; HGF, hepatic growth factor; HUVEC, human umbilical vein endothelial cell; IL-1β, interleukin-1β; MLC, myosin light chain; ROCK, Rho kinase; STED, stimulated emission depletion; STORM, stochastic optical reconstruction microscopy; TEER, transendothelial electric resistance.

The Rockefeller University Press $30.00
J. Cell Biol. Vol. 213 No. 3 385–402
www.jcb.org/cgi/doi/10.1083/jcb.201504038

ruffles in motile tumor cells (Palamidessi et al., 2008). To date, the role of Rac1 intracellular trafficking in the maintenance of endothelial barrier function has not been addressed.

Vascular injury is a hallmark of physiological and pathological inflammation. Prothrombotic proteases and inflammatory mediators induce acute endothelial hyperpermeability that can cause fatal vascular dysfunction (van Nieuw Amerongen et al., 1998; Levi et al., 2004). Among them, thrombin is of particular relevance in chronic inflammation because it can act synergistically with inflammatory cytokines, such as TNF, to modulate endothelial permeability (Tiruppathi et al., 2001) and to activate pathways implicated in the long-term inflammatory response (Levi et al., 2004; Liu et al., 2004). Thrombin is thus determinant in various pathological scenarios, including inflammatory bowel diseases, such as Crohn's disease (Saibeni et al., 2010). In general, acute endothelial contraction caused by thrombin and other inflammatory factors worsens pathologies related to chronic inflammation (Croce and Libby, 2007; Popović et al., 2012).

Here, in an expression screen for proteins up-regulated in endothelial cells during inflammation, we have found that RhoB protein levels are increased three- to fivefold in response to inflammatory cytokines. RhoB is expressed in small vessels from inflamed intestine or in endothelial beds with high permeability such as those in hepatic sinusoids. We show that RhoB, in conjunction with RhoA and RhoC, plays redundant and additive roles that control various aspects of endothelial barrier function, including ROCK-mediated signaling. In addition to this collaborative role, RhoB is specifically involved in sustaining acute contraction upon thrombin exposure in a context of inflammation. RhoB negatively regulates Rac1 activity and Rac1 intracellular trafficking during barrier recovery. This effect impairs the formation of plasma membrane extensions, inhibits barrier reformation, and makes endothelium persistently exposed to inflammatory cytokines less resistant to mediators that challenge the integrity of the endothelial monolayer.

Results

RhoB expression is increased in response to inflammatory cytokines and in vessels from human inflamed tissues

TNF reduces endothelial barrier integrity, which progressively increases vascular permeability to blood cells and small molecules through mechanisms that are not fully understood (Bradley, 2008). To identify new proteins regulating endothelial barrier function during the inflammatory response, we have combined quantitative PCR (qPCR), proteomics, and Western blotting to search for proteins whose expression is modulated by TNF. A time course of TNF or IL-1β stimulation in human umbilical vein endothelial cells (HUVECs) revealed that RhoB protein levels increase between 4 h and 24 h poststimulation, reaching a maximum fivefold increase for TNF and threefold increase for IL-1β compared with unstimulated cells (Fig. 1, A and B; and Fig. S1 A). No changes were detected in RhoA expression, whereas RhoC expression moderately increased in response to TNF. Primary human dermal microvascular endothelial cells (HDMVECs; Figs. 1 C and S1 B) and human endothelial cell lines (Fig. S1, C and D) also increased RhoB expression in response to TNF. The RhoB increment was moderate in epithelial cell lines (Fig. S1 D). RhoB localizes in endosomes, the cytosol, and the plasma membrane (Sandilands et al., 2004). Immunofluorescence analysis of endogenous RhoB showed that TNF increased RhoB expression mostly in a vesicular, endosomal-like compartment (Fig. 1, B and C). A qPCR analysis of HUVEC mRNA revealed a fourfold increase in RhoB mRNA and no significant changes in RhoA and RhoC mRNA in response to TNF (Fig. 1 D). In the whole Rho family, only the expression of Rnd1 mRNA was also significantly increased in response to TNF, whereas RhoH transcripts were not detected (Fig. S1 E). We quantified the relative expression levels of endogenous RhoA, RhoB, and RhoC proteins and found that they were similar in TNF-stimulated HUVECs (Fig. S1 F). The increase in GTP loading in response to TNF was moderate, with no statistical significance for each of the three Rho proteins (Fig. 1, E and F). The use of a panel of inhibitors suggested that TNF raises the level of RhoB expression mainly through a NF-κB–dependent pathway (Fig. S1, G and H). Therefore, these results indicate that RhoB expression increases upon long-term exposure to inflammatory cytokines. As a result, RhoA, RhoB, and RhoC are similarly expressed and activated in TNF-stimulated endothelial cells.

Immunohistochemical analysis showed that RhoB expression was weak in control umbilical cords (Fig. 2 A), in agreement with our results obtained in vitro from unstimulated HUVECs. RhoB expression was detected in some blood vessels from colon and small intestine tissue of patients with Crohn's disease (Fig. 2, B–D). Endothelial RhoB expression was localized in vessels in close proximity to fissures, the most inflamed and damaged areas of the tissue (Fig. S2, A–F; and Table S1), whereas vessels in the adjacent areas appeared negative (Fig. S2, A, D, and G–I) as did an isotype-specific control antibody (Fig. S2 J). RhoB-positive vessels were expressing low levels of the NG2 proteoglycan, suggesting that RhoB is highly expressed in postcapillary venules (Fig. 2, E–G). We also found RhoB expression in blood vessels irrigating inflamed ganglia in colon adenopathies associated with tumors (Fig. S2, K and L). We did not detect expression of RhoB in the endothelium of atheroma plaques from the carotid and aorta on in the normal small intestine (unpublished data). The liver parenchyma contains highly permeable vessels called sinusoids. RhoB was highly expressed not only in the sinusoidal endothelium from rejected human liver allografts and livers in advanced stages of hepatitis B virus infection but also in control donors (Fig. 2, H and I; and Table S1). Therefore, high levels of RhoB protein expression were detected in inflamed small blood vessels in human intestine and liver sinusoids, suggesting that RhoB protein levels are higher in endothelial beds with diminished barrier function.

A screening of endothelial barrier function reveals additive, redundant, and negative roles of the RhoA-subfamily proteins in unstimulated and TNF-stimulated HUVECs

The involvement of the Rho pathway in human cell barrier function has most often been addressed by inhibiting the entire RhoA protein subfamily or their common downstream effectors (McKenzie and Ridley, 2007; Fernández-Martín et al., 2012). Hence, we aimed to determine whether up-regulated RhoB plays a specific role in different barrier properties of human endothelial cells during inflammation (summarized in Table 1) by silencing the expression of each RhoA subfamily member with siRNA oligonucleotides (Fig. S3, A–D). Single and double Rho gene silencing induced expression changes in the remaining

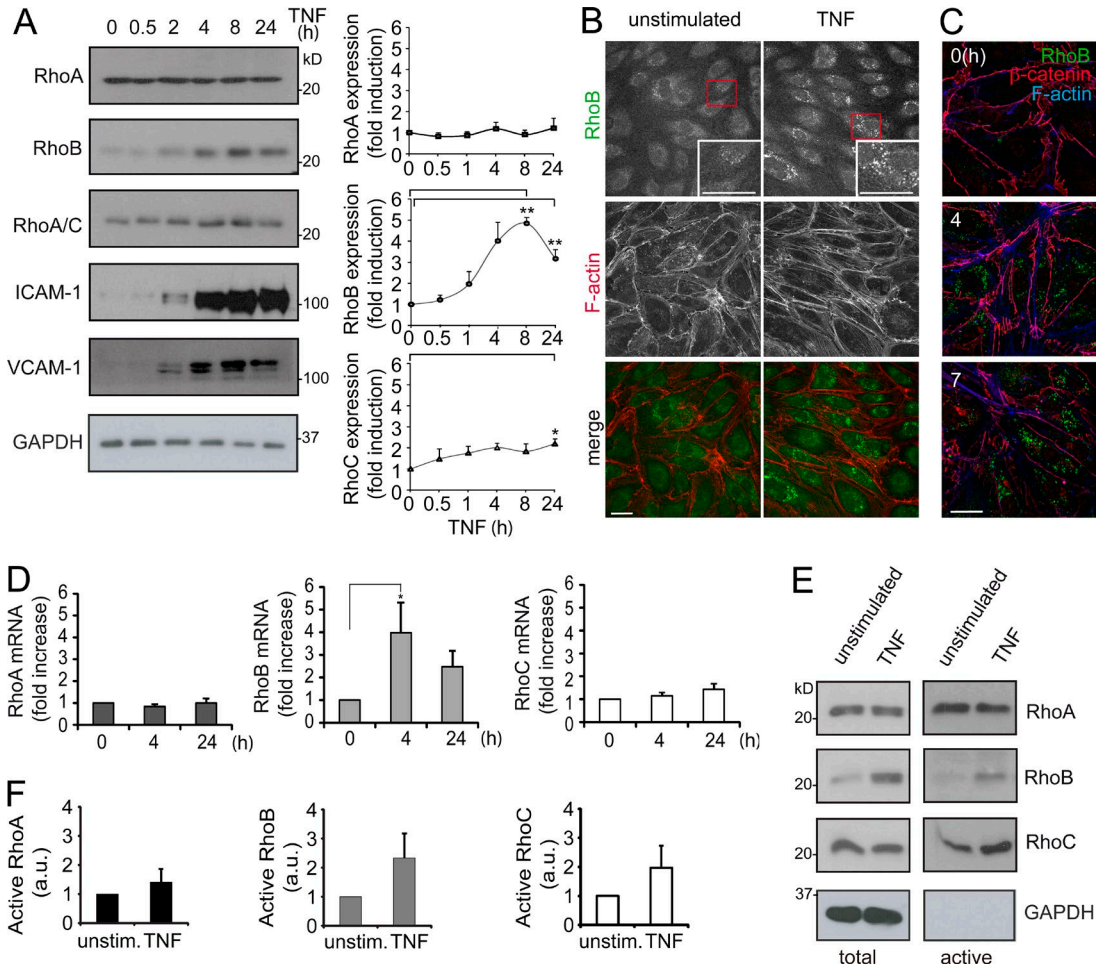

Figure 1. **RhoB is up-regulated in response to TNF in primary human endothelial cells.** (A) HUVECs were starved for 12 h and stimulated at different times with 10 ng/ml TNF. Right graphs quantify the expression changes of RhoA, RhoB, and RhoC in response to TNF. Mean + SEM of three different experiments. **, P = 0.001; *, P = 0.02 (B) HUVECs were left unstimulated or stimulated with TNF for 7 h, then fixed and stained with an antibody to RhoB and with phalloidin-TRITC to detect F-actin. TNF increased RhoB staining (enlarged areas). (C) HDMECs were stimulated with TNF at the indicated times and stained for the indicated proteins. (D) HUVECs were stimulated with TNF at different times, and RhoA, RhoB, and RhoC transcripts were analyzed by qPCR. Results were normalized to mRNA levels of β-actin and GADPH. Mean + SEM from four different experiments. Statistical significance tested for the three graphs *, P = 0.022. (E and F) Effect of 7-h TNF stimulation on active Rho proteins detected by pull-down assays. (F) Mean + SEM of six different experiments. No statistical significance with the Student's *t* test was found for any data comparison in the three graphs. Bars, 20 µm.

Rho proteins. RhoA depletion increased the expression of RhoB and RhoC by 2- to 2.5-fold, whereas single knockdown of RhoB increased RhoA and RhoC expression by 1.5- to 2-fold. Knockdown of RhoC moderately increased RhoA expression in TNF-stimulated and unstimulated cells, whereas reduced RhoB expression by 30% only in unstimulated HUVECs. Double reduction of Rho proteins caused a stronger compensatory increase in the expression of the remaining GTPases (Fig. S3, B and C). This suggests that RhoA, RhoB, and RhoC play additive or redundant roles in endothelial cells, which features mechanisms to modulate their expression and compensate for each other´s function. Indeed, individual depletion of RhoB and RhoC, but not RhoA, as well as the double Rho knockdown, decreased barrier function in unstimulated HUVECs, but this decrease was stronger upon triple Rho depletion (Fig. S3 E). These results suggest that RhoA, RhoB, and RhoC play additive roles in regulating constitutive endothelial barrier function. Electric cell substrate impedance sensing assays, which measures transendothelial electric resistance (TEER), and transwell permeability assays indicated that RhoC plays a predominant role in maintaining the integrity of the endothelial barrier in the absence of inflammatory stimuli (Fig. S3, E and F). We then examined the relative contribution of each Rho protein to the regulation of F-actin. Single Rho knockdown was not sufficient to reduce F-actin levels. In contrast, cells expressing only RhoB or RhoA, as well as cells depleted of the three GTPases, reduced them (Fig. S3, G and H). Collectively, these results indicate that these three GTPases play redundant roles in the regulation of F-actin. It is of note that cells expressing only RhoC had higher levels of F-actin, suggesting that RhoC expression is sufficient to mediate actin polymerization.

We investigated the role of RhoB in the endothelial barrier function of cells exposed to TNF. Single Rho protein depletion had no effect on permeability in cells stimulated with TNF between 7 and 24 h (Fig. 3, A and B). The F-actin levels and the T cell transendothelial migration were neither affected by individual Rho knockdown in TNF-stimulated HUVECs (Fig. S4, A–C). Discontinuous adherens junctions connecting actin stress fibers from adjacent cells regulate intercellular tension and are increased in response to TNF (Millán et

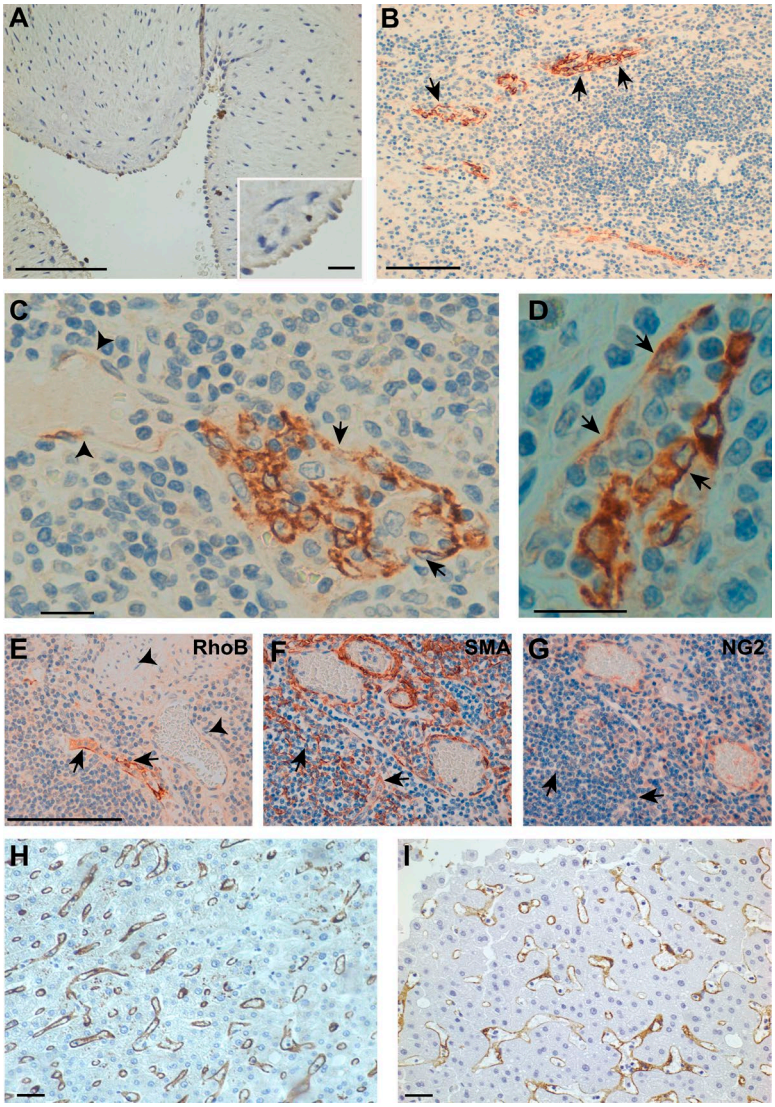

Figure 2. **RhoB is expressed in intestinal vessels of patients with Crohn's disease and hepatic sinusoids.** (A) Moderate immunohistochemical staining of RhoB from human umbilical veins. (B–D) Large intestine from a patient with Crohn's disease showing intense endothelial RhoB staining (arrows) in inflamed vessels containing high levels of adhered immune cells. (C and D) Differential RhoB staining, which suggests increased RhoB expression in vessel areas with high levels of leukocyte adhesion and capillary hyperplasia (arrows), with respect to areas with no immune cells (arrowheads; see Fig. S2). (E–G) Consecutive tissue sections showing that RhoB is preferentially expressed in small vessels positive for smooth muscle actin (SMA) and negative for the NG2 proteoglycan. (H and I) RhoB staining in sinusoids from a control liver (H) and hepatitis B virus–infected liver (I). Bars: (A, B, and E–I) 100 µm; (A, inset, and C and D) 10 µm.

al., 2010; Huveneers et al., 2012). The single reduction of each Rho protein had no apparent effect on the morphology of adherens junctions, whereas triple Rho knockdown turned them into linear junctions interspersed with big gaps (Fig. S4, A and B). Therefore, TEER and F-actin levels were reduced in TNF-stimulated cells simultaneously silenced for the three Rho GTPases, although this could not be attributed to a specific effect on TNF-mediated signaling because it was also observed before the TNF exposure (Fig. S3, G and H). However, the inhibition of ROCK, the main Rho downstream effector that controls actomyosin levels, did not prevent the reduction in TEER in TNF-stimulated cells (Fig. 3 A) as we had previously observed (McKenzie and Ridley, 2007; Fernández-Martín et al., 2012). This suggests that the RhoA GTPase subfamily has no significant role in long-term endothelial barrier disruption in response to TNF.

Table 1. **Functional screening of the effect of RhoA, RhoB, and RhoC siRNAs on the barrier properties of human primary endothelial cells**

Barrier analysis/siRNA	RhoA	RhoB	RhoC	RhoA/B/C
Unstimulated HUVECs				
Constitutive barrier function	−/+	+	++	+++
F-actin levels	−	−	−	+++
TNF-stimulated HUVECs				
TNF-induced barrier dysfunction	−	−	−	ND
TNF-induced F-actin increase	−	−	−	+++
Leukocyte transendothelial migration (static)	−	−	−	−
Acute cell contraction	−/+	+	−/+	+++
Barrier restoration after contraction	−	+++	−/+	+++

ND, not determined.

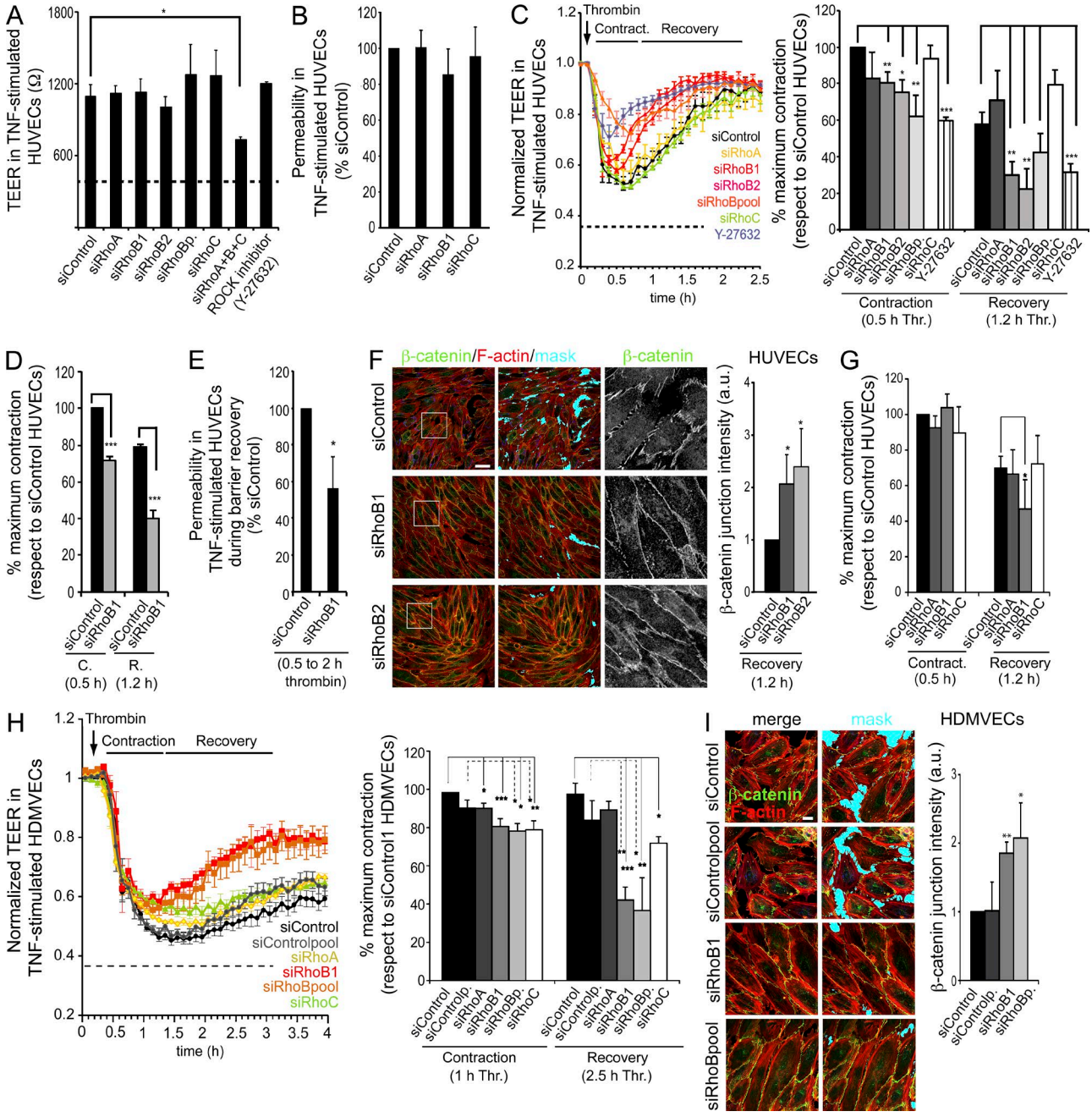

Figure 3. **RhoB negatively regulates endothelial barrier recovery after acute contraction human endothelial cells.** (A and B) Single knockdown of RhoA, RhoB, and RhoC has no effect on the barrier function of TNF-stimulated HUVECs. (A) Absolute TEER of HUVECs transfected with the indicated siRNA oligonucleotides for 72 h or incubated with TNF for 7 h. Control cells were incubated with 5 µm Y-27632 for 30 min before TNF stimulation when specified. Discontinuous line marks the basal resistance values in empty electrodes. *, $P < 0.5$. RhoBp, RhoB pool. (B) Permeability to dextran-FITC of siRNA-transfected HUVECs plated on transwells for 48 h and stimulated with TNF. No statistically significant differences were found in permeability values between siControl and siRho-transfected cells. (C) Left graph shows changes in TEER during thrombin-induced acute contraction in cells pretreated with TNF for 7 h as in A. Mean ± SEM from at least three independent experiments. (right graph) Percentage of maximum contraction with respect to siControl cells during acute contraction (0.5 h of thrombin stimulation) and barrier recovery (1.2 h of thrombin stimulation). A total of 5 µM Y-27632 was added 30 min before thrombin stimulation when indicated. Mean + SEM from at least three independent experiments. *, $P < 0.02$; **, $P < 0.007$; ***, $P < 10^{-3}$. (D) Percentage of maximum contraction with respect to siControl cells during acute contraction (C.) and barrier recovery (R.) in HUVECs pretreated with TNF between 18 and 20 h. ***, $P < 2.2 \times 10^{-5}$. (E) Permeability to dextran-FITC was performed as in B but analyzed during the time of barrier recovery after acute contraction induced by thrombin. (F) Staining for β-catenin and F-actin in TNF-pretreated HUVECs stimulated during the recovery phase after thrombin. Empty spaces between cells were identified by automated image analysis (mask). β-Catenin staining at cell borders was quantified by semiautomated image processing in five different experiments. *, $P \leq 0.046$. Bar, 20 µm. (G) Percentage of maximum contraction with respect to siControl cells during acute contraction and the subsequent recovery induced with thrombin in HUVECs not previously stimulated with TNF. *, $P = 0.047$; **, $P = 0.009$; ***, $P = 9.4 \times 10^{-5}$. (H) Changes in TEER during thrombin-induced acute contraction in HDMVECs pretreated with TNF for 7 h (left). Mean ± SEM from at least three independent experiments. Percentage of maximum contraction with respect to siControl1 during contraction and barrier recovery in HDMVECs (right). *, $P \leq 0.05$; **, $P < 0.01$; ***, $P < 0.005$. (I) TNF-pretreated HDMVECs were fixed after 2.5 h of thrombin stimulation (recovery phase) and stained for β-catenin and F-actin. β-Catenin staining at cell borders was quantified as in F. *, $P < 0.05$; **, $P < 0.01$. Bar, 10 µm. Mean + SEM of at least three experiments.

RhoB sustains acute contraction and delays endothelial barrier recovery in TNF-stimulated HUVECs

Inflammation and coagulation influence each other in chronic inflammatory pathologies such as Crohn's disease, ulcerative colitis, and multiple sclerosis (Scaldaferri et al., 2011; Roshanisefat et al., 2014). Thrombin-mediated activation of protease-activated receptors is a paradigm of acute Rho-controlled actomyosin-dependent contraction that disrupts endothelial integrity and causes vascular dysfunction in a range of proinflammatory diseases (Croce and Libby, 2007; Borissoff et al., 2009). Thus, we next investigated whether TNF–up-regulated RhoB expression contributes to acute barrier disruption induced by thrombin in an inflammatory context. The barrier function of TNF-pretreated, single siRNA–transfected HUVECs was analyzed after thrombin stimulation. Before thrombin, no significant changes in TEER were observed in these cells (Fig. 3 A). Thrombin induced a rapid and acute decrease in TEER, followed by a slower recovery to initial values of resistance (Fig. 3 C, left graph). Control siRNA or siRNA targeting RhoA and RhoC had no major effect on TEER. RhoB was silenced with two individual siRNAs, as well as with a pool of four different and specific RhoB siRNAs designed to reduce off-target effects (Fig. S3, A–D). The three sets of RhoB siRNA inhibited the initial reduction of TEER 30 min after thrombin stimulation (maximum contraction) and significantly shortened the subsequent monolayer recovery time, quantified by measuring TEER recovery 72 min after thrombin stimulation (Fig. 3, C [right] and D; and Fig. S3, A–D). This was similar to the effect that we and others had observed by ROCK inhibition (Fig. 3 C; Kawkitinarong et al., 2004; Fernández-Martín et al., 2012), although Y27632 had a stronger effect on initial contraction. RhoB-depleted cells also had reduced permeability when analyzed by transwell permeability assays during the period of time between acute contraction and barrier recovery (Fig. 3 E). RhoB knockdown increased cell–cell junction integrity, which was addressed by localizing β-catenin after thrombin stimulation (Fig. 3 F, right graph). RhoB knockdown had a specific but milder effect on endothelial barrier reformation in HUVECs not previously treated with TNF and, therefore, with lower levels of RhoB protein (Fig. 3 G). Finally, in HDMVECs, single Rho knockdown induced a moderate decrease in acute contraction, whereas barrier recovery was also accelerated by RhoB depletion and at less extent, by RhoC depletion (Fig. 3 H and Fig. S3, A and D). HDMVEC barrier reformation was increased upon RhoB knockdown when analyzed by confocal analysis of cell–cell junction integrity (Fig. 3 I), indicating that RhoB also plays a specific role in prolonging thrombin-induced barrier disruption in microvascular endothelial cells.

Thrombin stimulation activated RhoA, RhoB, and RhoC with comparable kinetics in HUVECs pretreated with TNF (Fig. 4, A and B). Because expression levels were also similar (Fig. S1 F), we hypothesized that RhoB specificity on prolonging cell contraction could be caused by the differential regulation of downstream signaling pathways involved in this process. Active Rho can increase myosin light chain (MLC) phosphorylation through ROCK activation (Riento and Ridley, 2003). This promotes nonmuscle myosin II isoforms to interact with F-actin and to increase actomyosin contractility. Depletion of RhoA, but not RhoB, reduced MLC phosphorylation 2 min after thrombin stimulation (Fig. 4, C and D). Paxillin is a scaffolding protein that regulates focal adhesion (FA) stability and becomes phosphorylated upon interaction with other FA components, including FA kinase, reported to be essential for endothelial barrier restoration after thrombin stimulation (Knezevic et al., 2009). Single RhoA and RhoB knockdown similarly reduced paxillin phosphorylation in Tyr-31, which suggested no selective role for RhoB in regulating this protein (Fig. 4, C and E). These results suggest that RhoB's specific role in endothelial barrier recovery does not involve signaling to MLC and paxillin and that partial inhibition of MLC activation is not sufficient to prevent thrombin-induced contraction.

RhoB prevents endothelial plasma membrane extension after acute contraction

We observed that the expression of a constitutive active mutant RhoB-V14 had no effect on cell–cell junction integrity even though cell-spread area was significantly reduced (Fig. 5 A). This led us to hypothesize that the role of RhoB in thrombin-mediated endothelial remodeling may be independent of the reannealing of cell–cell junctions. Indeed, the kinetics of thrombin-induced contraction and subsequent spreading in TNF-pretreated subconfluent HUVECs were consistent with those of barrier disruption and reformation in confluent cells, indicating that cell contraction and recovery are independent of the cell–cell junctions (Figs. 3 C and 5 B). Confocal analysis revealed that RhoB knockdown slightly increased cell area of subconfluent HUVECs before thrombin stimulation and clearly accelerated cell respreading after thrombin-mediated contraction (Fig. 5 C). 60 min after thrombin stimulation, RhoB-depleted cells recovered their initial spreading area, whereas siControl cells had only 60% of their area before stimulation (Fig. 5 C). In contrast, RhoB-V14 expression reduced cell respreading (Fig. 5 D), suggesting that RhoB negatively regulates the membrane extension that follows acute contraction. A similar increase in cell area was observed in RhoB-depleted subconfluent HDMVECs at the time of cell respreading (Fig. 5 E).

Time-lapse confocal analysis of GFP-RhoB revealed that the number of RhoB-positive vesicles moving between an endosomal-like perinuclear compartment and the plasma membrane more than doubled during membrane reextension after thrombin-induced contraction, compared with cells before contraction (Fig. 6, A–C; and Videos 1 and 2). This increase was detected in both directions, from the perinuclear compartment toward the plasma membrane (Fig. 6 B) as well as for vesicles that emerge from the plasma membrane and follow inward movement (Fig. 6 C). In addition, the analysis of endogenous RhoB distribution by superresolution microscopy revealed that RhoB was not evenly distributed but formed nanoclusters in the endosomal vesicles (Fig. 6 D), which were modestly reduced in response to thrombin (Fig. 6 E). To identify the intracellular localization of RhoB, we analyzed the distribution of endogenous RhoB with respect to different endosomal markers. RhoB has been localized in an early endosomal compartment (Fernandez-Borja et al., 2005; Kroon et al., 2013). TNF-stimulated HUVECs were loaded with transferrin-TRITC for 5 min before performing a time course of thrombin stimulation. A small fraction of RhoB vesicles overlapped with transferrin suggesting a partial localization of RhoB in early endosomes (Fig. 6 F and not depicted). This was confirmed by colocalization analysis in cells expressing the early endosomal GFP-Rab5, in which some vesicles overlapped with RhoB at any time of thrombin stimulation (Fig. 6 F and not depicted). The partial overlap between RhoB and transferrin was reduced in cells stimulated with

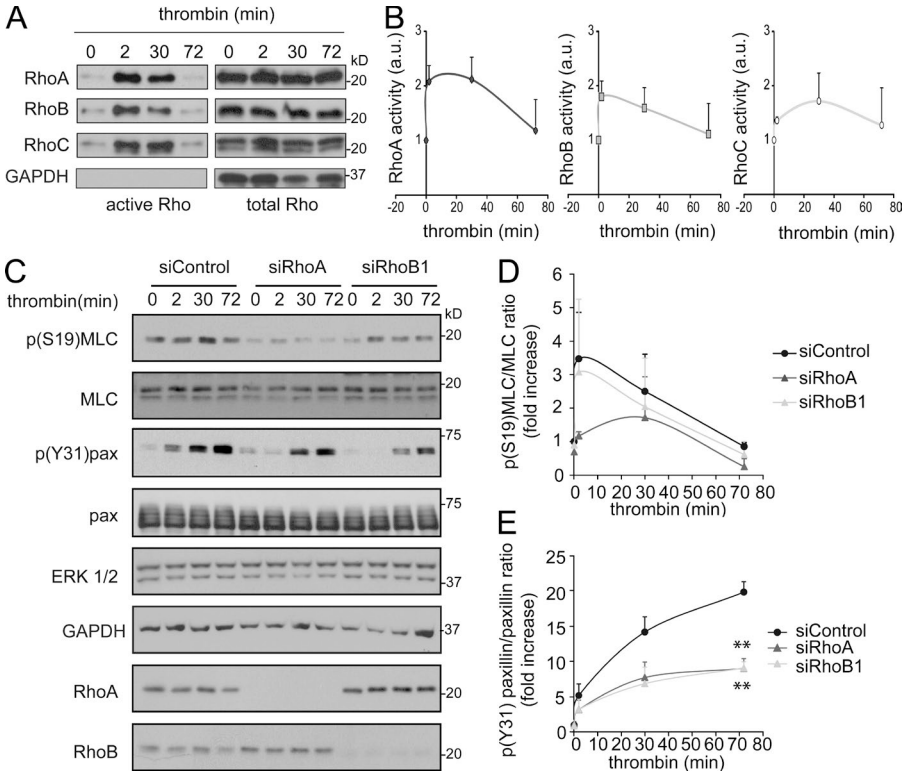

Figure 4. **Effect of RhoA and RhoB on myosin light chain and paxillin phosphorylation.** (A) Pull-down assays of RhoA, RhoB, and RhoC during acute contraction induced with thrombin in HUVECs pretreated with TNF for 8 h. Graphs show active Rho normalized to total Rho levels from three different experiments. (B) TNF-pretreated, siRNA-transfected HUVECs were stimulated with thrombin for the indicated times and immunoblotted for the indicated proteins. (C and D) Quantification of phosphorylation of the indicated proteins from at least three experiments. **, $P < 0.005$.

thrombin and simultaneously loaded with transferrin for 1.2 h, which suggests that RhoB does not significantly localize in an endosomal-recycling compartment during barrier recovery (Fig. 6 F). RhoB colocalization with recycling GFP-Rab11 was also minor at any time of thrombin stimulation (Fig. S5 A and not depicted). Similarly, the colocalization of RhoB vesicles with the fast-recycling Rab4 and the protein epsin homology domain 1 (EHD-1), which regulates specific trafficking pathways in the recycling system (Goldenring, 2015), was negligible (Fig. S5 A). In contrast, RhoB perinuclear clusters and vesicles colocalized with the late endosomal marker Rab7, suggesting that RhoB distributes along the endocytic route between early and late endosomes, but mainly in this latter compartment, as previously described for epithelial cell lines (Wherlock et al., 2004).

RhoB negatively regulates Rac1 trafficking from the endosomal compartment to the plasma membrane

The Rho GTPase Rac1 plays a central role in regulating plasma membrane extension (Price et al., 1998) and endothelial permeability and cell–cell junction stabilization (Daneshjou et al., 2015). We investigated whether RhoB regulates Rac1-mediated cell spreading. Exogenous expression of Rac1 was sufficient to induce membrane extensions and increase the cell-spread area HEK293 cells. Interestingly, coexpression of RhoB-V14 impaired Rac1-induced protrusions in cells expressing similar levels of exogenous Rac1 (Fig. S5 B). Thus, active RhoB impairs the plasma membrane extension after thrombin stimulation, but also upon Rac1 overexpression. The extension of the plasma membrane during cell migration requires Rac trafficking between the plasma membrane and a Rab5-positive endosomal compartment, in which Rac encounters and recycles with guanine nucleotide exchange factors toward the plasma membrane to form F-actin–mediated protrusions (Palamidessi et al., 2008). We analyzed the distribution of Rac1 in endothelial cells and found it to be localized at the plasma membrane and in internal vesicular clusters (Fig. 7 A). Expression of constitutively active RhoB-V14 significantly reduced Rac1 localization in the plasma membrane, even in cells that were properly spread and adhered to the substrate (Fig. 7 A). In contrast, reduction of RhoB expression increased Rac1 localization at cell borders (Fig. 7 B). Moreover, Rac1 and RhoB-V14 clearly colocalized in a perinuclear vesicular compartment positive for Rab7 (Fig. 7, C and D) and in a compartment positive for Rab5 (Fig. 7, C and E). The localization of active RhoB-V14 in Rab5-positive endosomes increased with respect to exogenous or endogenous RhoB (Figs. 6 F and 7 E). Endogenous RhoB staining also overlapped with Rac1 in an intracellular compartment in confluent HUVECs (Fig. 7 F) and in HDMVECs (Fig. S5 C) pretreated with TNF. During barrier reformation after thrombin stimulation, Rac1 and RhoB partially colocalized in vesicles, but not in lamellipodial-like extensions (Fig. 7 F). Therefore, RhoB activity reduces Rac1 presence at the cell border and favors Rac1 intracellular localization.

However, superresolution confocal microscopy suggested that Rac1 and RhoB accumulate in different domains in intracellular vesicles (Fig. 7 G). Accordingly, no association was detected between Rac1 and RhoB in coimmunoprecipitation experiments and in the pull-down assays performed to analyze Rac1 and RhoB activity (unpublished data). We then investigated whether RhoB and Rac1 could be in proximity and therefore establish transient but undetectable interactions. We generated a construct of RhoB conjugated from its N-terminal domain to the mutant of biotin-ligase BirA, which adds biotin to proteins in its proximity, and performed BioID assays (Fig. 7 H; Roux et al., 2012). GFP-Rac1 coexpressed with RhoB-BirA was detected in pull-down assays performed with neutravidin to purify biotinylated proteins (Fig. S5 D). Exogenous biotin was required for GFP-Rac1 biotinylation, whereas GFP alone was

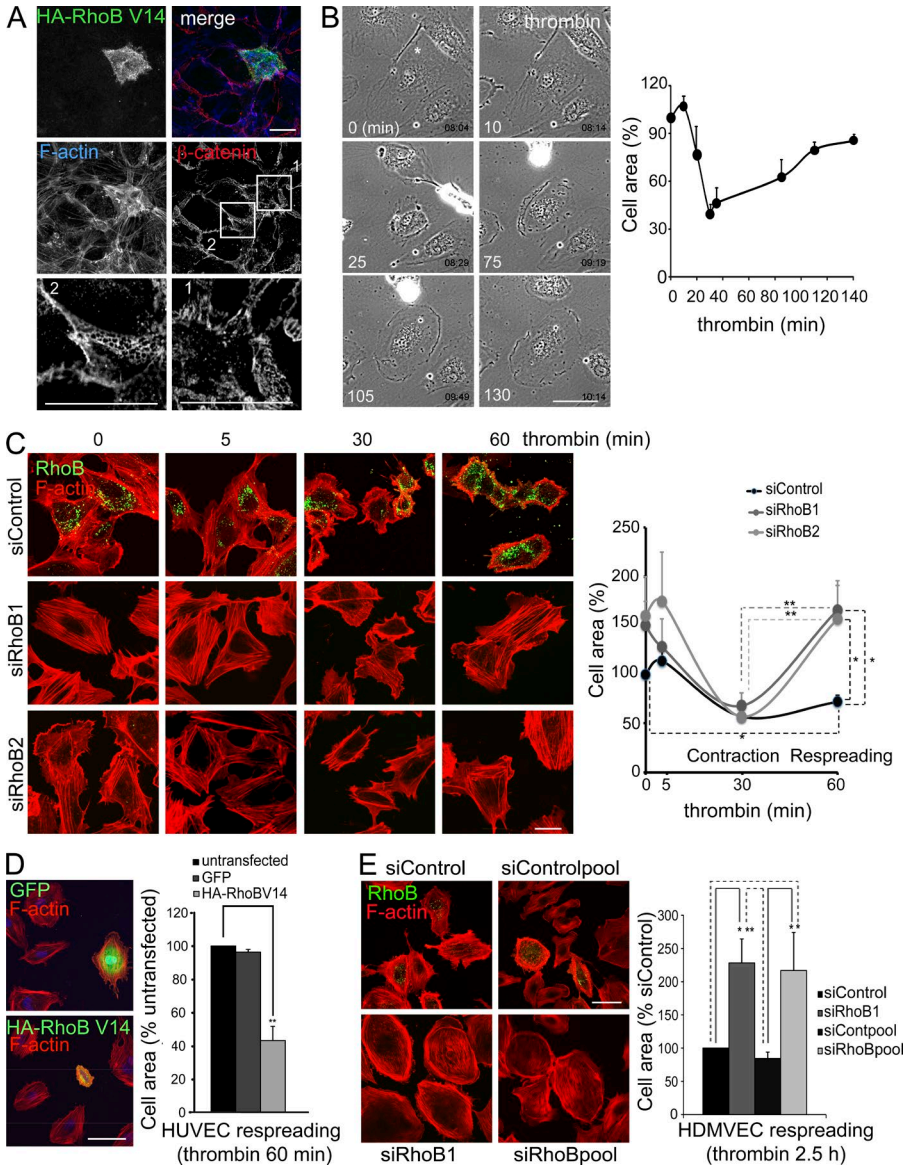

Figure 5. **RhoB regulates cell area recovery after acute contraction independently of cell–cell contacts.** (A) HA-RhoBV14 has no effect on endothelial cell–cell junctions. HA-RhoBV14 was expressed for 48 h in confluent HUVECs. Bottom images show enlargements of squared areas from HA-RhoBV14 transfected (1) and untransfected cells (2). Bar, 20 µm. (B) Time-lapse microscopy of subconfluent HUVECs stimulated with thrombin. Cell areas were quantified from individual frames taken at different times (right graph). Graph shows the mean + SEM of at least 10 cells per experiment from three different experiments. Bar, 20 µm. (C) siRNA-transfected, TNF-pretreated HUVECs were stimulated with thrombin for the indicated times, and then fixed and stained for F-actin and RhoB. Right graph quantifies cell area. Mean + SEM from three different experiments. 50 cells per experiment. RhoB-depleted cells recover their initial area (respreading) at 60 min poststimulation. *, $P < 0.04$; **, $P < 0.03$. (D) HUVECs expressing GFP or HA-RhoBV14 for 24 h were stimulated with thrombin for 60 min, stained for F-actin and HA-RhoBV14, and the cell area quantified. Graph shows the mean + SEM of at least 10 cells per experiment from three different experiments. **, $P = 0.001$. (E) siRNA-transfected, TNF-pretreated HDMVECs were stimulated with thrombin for 2.5 h (respreading), and then fixed and stained for F-actin and RhoB. Graph shows the mean + SEM from at least 50 cells per experiment, from three different experiments. *, $P \leq 0.05$; **, $P < 0.01$. Bar, 10 µm.

not biotinylated (Fig. S5 E). Overexpression of RhoB-BirA induced a reduction of GFP-Rac1 expression compared with cells expressing only GFP-Rac1 (Fig. S5 D and Fig. 7 H). We then adopted a complementary strategy and immunoprecipitated Rac1 in the presence or absence of BirA-RhoB. Cells expressing BirA-RhoB induced biotinylation of several proteins, which were detected by blotting with streptavidin conjugated to peroxidase (Fig. 7 H). At least four biotinylated proteins were found in the GFP-Rac1 immunoprecipitates (Fig. 7 H, asterisks). Two of these proteins were coincident with those detected by Western blot using anti-Rac1 antibody, which corresponded to the molecular weights of GFP-Rac1 and endogenous Rac1, which coimmunoprecipitated with GFP-Rac1 (Fig. 7 H).

Consistent with the role of RhoB in Rac1 localization, time-lapse confocal microscopy revealed that RhoB knockdown reduced the number of Rac1 vesicles moving toward and away from the plasma membrane and induced the accumulation of Rac1 at the periphery (Fig. 7, I and J; and Videos 3 and 4). Together, these results indicate that active RhoB transiently colocalizes with and retains Rac1 in an endosomal compartment, preventing it localizing to the plasma membrane.

RhoB inhibits endothelial barrier restoration by controlling Rac1 activity and trafficking

Simultaneously with RhoA and RhoB activation, Rac1 activity decreases within the first minutes of thrombin stimulation and subsequently recovers (Fig. 8 A). Pull-down assays during a time course of thrombin stimulation showed an increase in Rac1 activity in RhoB-depleted HUVECs with respect to control cells at the time of cell respreading (Fig. 8 A). Rac1 activity did not change in RhoA-depleted cells (Fig. 8 B). Transient inhibition of Rac activity with NSC23766 during the time of barrier recovery abolished the effect of RhoB siRNA (Fig. 8, C and D), suggesting that Rac mediates the role of RhoB in sustaining cell contraction in endothelial monolayers. Next, we addressed whether Rac1 trafficking is involved in barrier restoration. Brefeldin A is a lactone antibiotic that inhibits anterograde intracellular transport and induces tubulation of the endosomal system (Lippincott-Schwartz et al., 1991), monensin is a ionophore that increases the pH of acidic endosomal vesicles and blocks their transport (Chapman and Munro, 1994), and dynasore impairs vesicle endocytosis and recycling

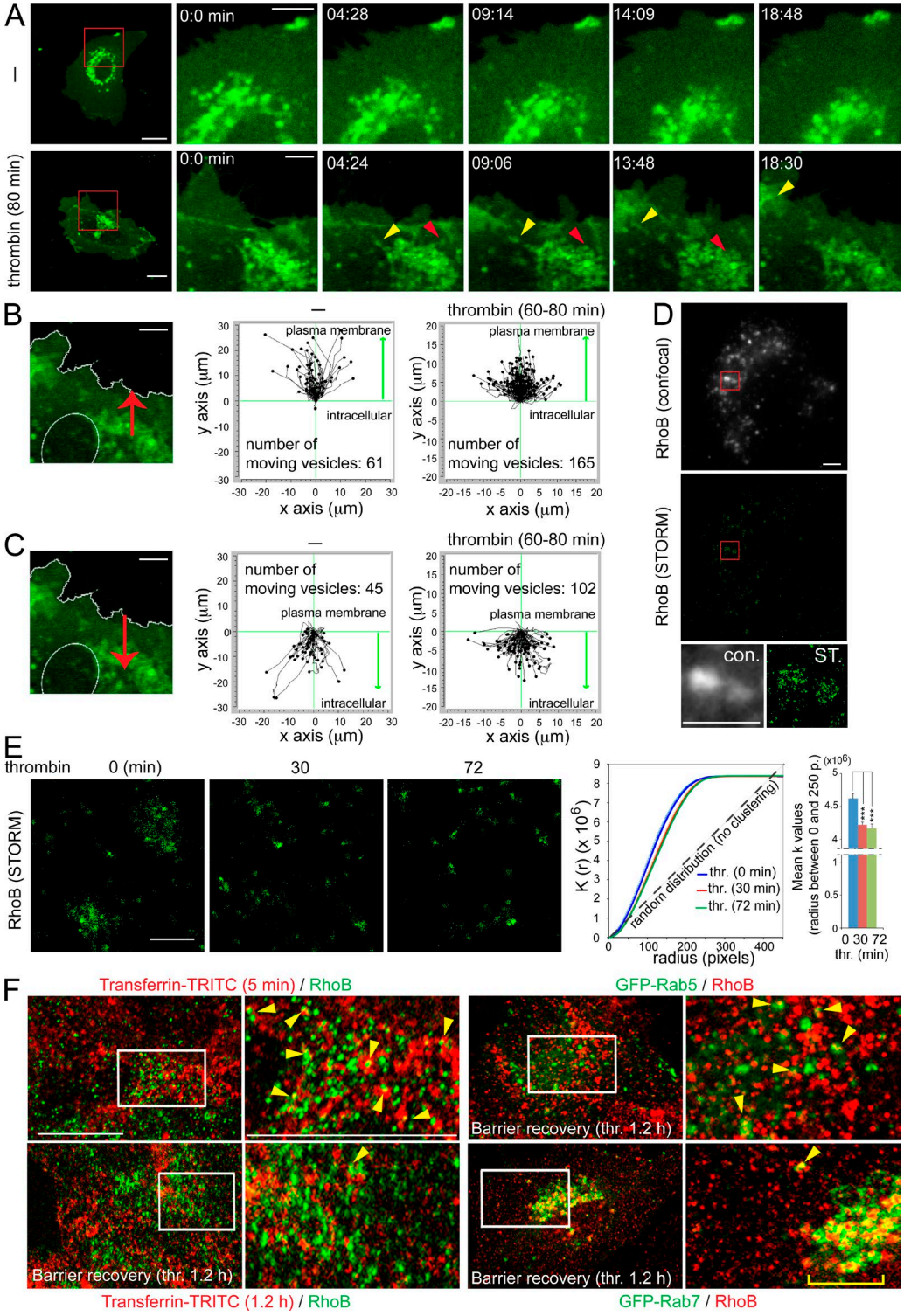

Figure 6. **Thrombin increases RhoB vesicular trafficking and reduces vesicular RhoB nanoclusters during cell area recovery.** (A–C) GFP-RhoB was expressed in HUVECs for 24 h. TNF-pretreated cells were left unstimulated (–) or stimulated with thrombin for at least 60 min and analyzed by time-lapse confocal microscopy at 20-s intervals during a 20-min period. Bars: 20 µm; (zoom) 2 µm. (B) RhoB-positive vesicles emerging from a perinuclear compartment toward the plasma membrane were tracked and the tracks plotted with a common origin. 12 cells per condition were analyzed. Bar, 2 µm. (C) RhoB-positive vesicles emerging from the plasma membrane toward a perinuclear compartment were tracked and the tracks plotted with a common origin. 12 cells per condition were analyzed. Bar, 2 µm. (D) STORM microscopy to generate a superresolution image of RhoB in perinuclear vesicles in TNF-pretreated HUVECs. Bar, 2 µm. (E) STORM images of RhoB clusters in intracellular vesicles during thrombin stimulation in TNF-pretreated HUVECs. Pixels of the reconstruction are shown. RhoB clustering was measured by calculating the Ripley´s K-function. K function for clusters from at least five images in three different experiments was calculated. ***, $P < 0.005$. Bar, 2 µm. (F) Localization of endogenous RhoB in TNF-pretreated HUVECs previously incubated with transferrin-TRITC for 5 min to localize early endosomes and for 1.2 h to localize recycling endosomes during barrier recovery. Localization of endogenous RhoB upon expression of the indicated Rab-GFP proteins. RhoB clearly colocalizes with Rab7-positive vesicles (arrowhead) in a perinuclear compartment (bracket).

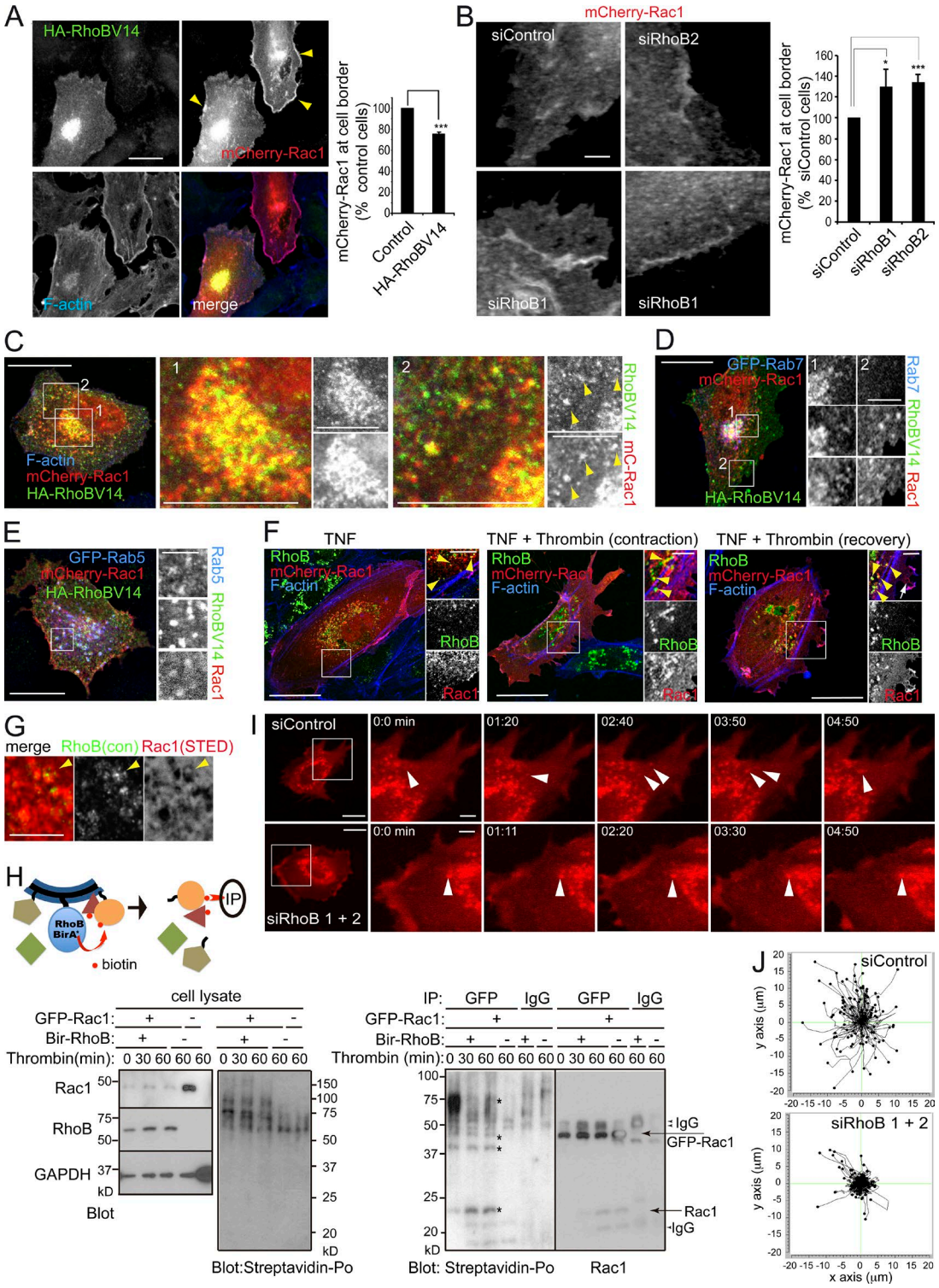

Figure 7. **RhoB regulates endothelial Rac1 localization and trafficking.** (A) mCherry-Rac1 and HA-RhoBV14 were expressed in EA.hy.926 cells and stained for HA epitope and F-actin. Right graph quantifies relative mCherry-Rac1 localization at cell border and shows the mean + SEM of at least 10 cells per experiment quantified in three different experiments. Arrowheads point to mCherry-Rac1 at the plasma membrane. RhoBV14 reduces Rac1 border localization even in cells correctly spread on the substrate. ***, $P = 5.30 \times 10^{-5}$. (B) HUVECs were transfected with the indicated siRNAs and then mCherry-Rac1 expressed during the last 24 h. TNF-pretreated cells were stimulated with thrombin for 60 min and fixed, and mCherry-Rac1 was quantified as in A. Graph shows the mean + SEM of four experiments. *, $P = 0.026$; ***, $P = 5 \times 10^{4}$. (C) mCherry-Rac1 colocalizes with active RhoB in intracellular compartments. mCherry-Rac1 and HA-RhoBV14 were expressed in EA.hy.926 cells. Significant colocalization was observed in a perinuclear compartment (1) and in a dispersed vesicular pattern (2; arrowheads). (D and E) HA-RhoBV14 and mCherry-Rac1 co localize in Rab5-GFP (D) and Rab7-FGP–positive (F) compartments. Right images show an enlargement of the squared area. (F) Endogenous RhoB and mCherry-Rac1 partly colocalize in a vesicular compartment in confluent, TNF-pretreated HUVECs stimulated or not with thrombin for 30 and 72 min (arrowheads). mCherry-Rac1 is also localized in nascent membrane protrusions (arrowhead). Bars: (A–F) 20 µm; (D–F, enlarged areas) 5 µm. (G) STED confocal images of Rac1 clusters, which appear different to those of RhoB in the same vesicle (arrowhead). Bar, 4 µm (H) BioID assay with BirA-RhoB. HEK293 cells were transfected with BirA-RhoB and

by inhibiting dynamin-2, a GTPase involved in clathrin-coated vesicle formation (Macia et al., 2006). We found that brefeldin A, monensin, and dynasore decreased barrier reformation and caused intracellular accumulation of Rac1 (Fig. 9, A, B, and E). In addition, brefeldin A reduced the movement of Rac1-positive intracellular vesicles (Fig. S5, F and G; and Videos 5 and 6). Conversely, hepatocyte growth factor (HGF) induces Rac1 translocation from the Rab5 compartment to the plasma membrane in nonendothelial cells (Palamidessi et al., 2008). Exposure of thrombin-stimulated endothelial cells to HGF at the initiation of monolayer recovery increased Rac1 translocation to the plasma membrane and, accordingly, accelerated barrier function recovery (Birukova et al., 2007; Fig. 9, C-E), similar to the effect of RhoB knockdown. Together, our results indicate that RhoB negatively regulates the endothelial membrane extensions required for barrier reformation, which are controlled by Rac1 trafficking.

Finally, we had previously shown a milder effect of RhoB siRNA on endothelial barrier recovery in the absence of long-term TNF stimulation, in which RhoB is expressed at low levels (Fig. S5 A). NSC23766 moderately delayed barrier reformation in unstimulated cells but caused strong and sustained inhibition of barrier reformation at least 4 h after thrombin stimulation in TNF-pretreated cells (Fig. 9 F). These results suggest that RhoB and Rac1 contribute to endothelial barrier recovery primarily in an inflammatory context.

Discussion

To investigate the molecular mechanisms mediating endothelial barrier dysfunction, we searched for new proteins whose expression is modulated by TNF. We found that TNF and IL-1β increased RhoB mRNA and protein expression in HDMVECs and HUVECs, which is comparable to what was recently reported in HUVECs (Kroon et al., 2013). In addition, RhoB is highly expressed in some vessels from chronically inflamed tissues, such as those in lesions from patients with Crohn's disease, and in leaky and specialized vessels, such as hepatic sinusoids. RhoB belongs to the RhoA subfamily, which regulates common effectors that are potential targets for treating proinflammatory and prothrombotic diseases and ameliorating endothelial dysfunction (Shi and Wei, 2013). For this reason, we undertook a detailed analysis of the role of each subfamily member in this regulation in human primary endothelial cells. Our functional analyses by transient gene silencing reveal first that RhoA, RhoB, and RhoC play additive roles in maintaining homeostatic barrier function and junction distribution and redundant or compensatory roles in regulating F-actin levels. The additive roles of RhoA and RhoB in endothelial barrier function have also been observed by expressing dominant-negative (DN) forms of RhoA and RhoB (Wojciak-Stothard et al., 2012). Single expression of the DN mutant of RhoA significantly inhibited the increase in pulmonary endothelial permeability noted under hypoxic conditions, whereas no significant effect was detected upon expression of DN RhoB. Coexpression of both DN mutants increased their inhibitory effect, suggesting that RhoB cooperates with RhoA in controlling endothelial barrier disruption during hypoxia (Wojciak-Stothard et al., 2012). DN Rho proteins inhibit endogenous Rho proteins by sequestering upstream GTP exchange factors, so their DN effect is extended to those Rho proteins that share these activators (Feig, 1999). Hence, their specificity with respect to the other two members of the family may be reduced compared with gene-silencing–based strategies. Our data indicate that among those additive effects, RhoC plays a main role in controlling constitutive endothelial barrier function whereas RhoB seems to have a predominant role in mediating acute contraction in endothelial cells exposed to inflammatory mediators. The analyses of a knockout mouse model of RhoB and the gene silencing of RhoC in human endothelial cells have previously shown the importance of RhoB and RhoC for other endothelial functions related to barrier function such as angiogenesis (Gerald et al., 2013; Hoeppner et al., 2015), whereas the study of the vascular-specific RhoA knockout mouse indicate that this GTPase is essential for mediating the permeability increase in response to histamine (Mikelis et al., 2015). However, no comparative studies of the relative expression and contribution of other RhoA subfamily members have been reported in these studies.

Thrombotic factors can cause endothelial contraction leading to a disruption of vascular integrity during inflammation (Beckers et al., 2010). Whereas contraction can be partially inhibited by inhibitors that target the common downstream effector ROCK (Komarova et al., 2007; Fernández-Martín et al., 2012), we have identified a novel and specific function for RhoB as a negative regulator of barrier reformation through the control of Rac1 localization and activity. This negative regulation occurs in cytokine-pretreated vascular and microvascular endothelial cells, but it is also detected in endothelial cells that are not pretreated with cytokines in which the effect of RhoB siRNA is milder than in TNF-stimulated cells, consistent with the relatively low level of expression of RhoB in the absence of inflammatory stimulation. Therefore, on the one hand, RhoB has similar roles to those of RhoA and RhoC, for instance, in regulating F-actin, whereas RhoB specifically mediates endothelial barrier reformation and controls Rac1 intracellular trafficking. This dual role might reflect the fact that RhoB is the only member of this subfamily that undergoes alternative lipid modifications in its C-terminal domain. Similar to RhoA and RhoC, a subset of RhoB is geranylgeranylated and localizes at the plasma membrane in its active form, whereas another subset of RhoB molecules, but not of RhoA and RhoC molecules, is isoprenylated and palmitoylated, which specifically localizes that GTPase at the endosomal compartment (Wheeler and Ridley, 2004; Pérez-Sala et al., 2009).

Rac1 targeting to the cell border from an endosomal compartment was found to be necessary to form actin-mediated plasma-membrane protrusions during cell migration, and HGF

GFP-Rac1 when indicated. GFP-Rac1 was immunoprecipitated with anti-GFP antibodies. Biotinylated proteins were detected by blotting with streptavidin peroxidase (asterisks). IgG, isotype-specific antibody control. Coexpression of BirA-RhoB reduces GFP-Rac1 detection in the cell lysates. (I) mCherry-Rac1 was expressed for 24 h in siRNA-transfected HUVECs. TNF-pretreated cells were stimulated with thrombin between 60 and 100 min, and Rac1 vesicular movement was recorded at 15-s intervals during a minimum of 5 min. Arrowheads point to mCherry-Rac–positive vesicles. In the top row of images, one vesicle divides in two and merges again. Bars: 20 µm; (zoom) 2 µm. (J) Each graph represents the tracks of 15 vesicles per cell, in eight cells, from three different experiments. Vesicle tracks were plotted with a common origin.

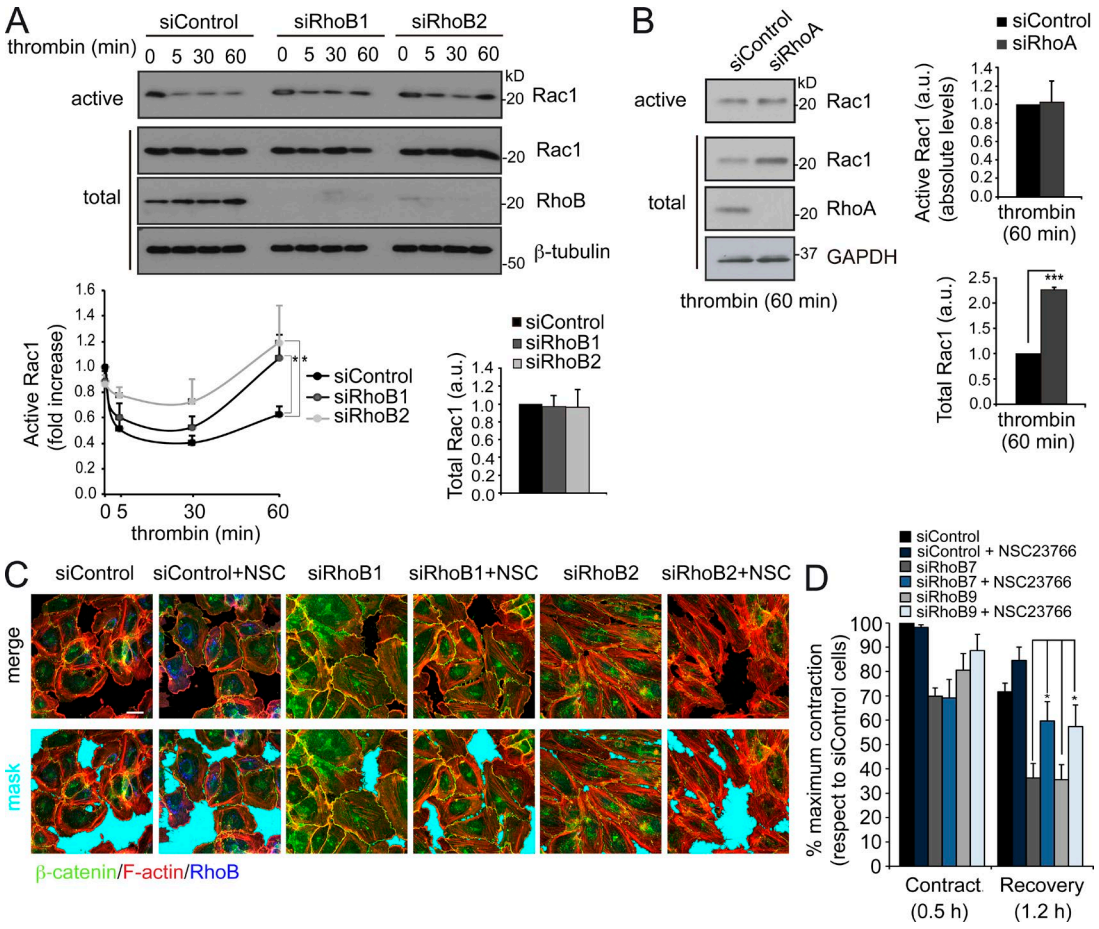

Figure 8. **Rac1 activity is regulated by RhoB and is required for endothelial barrier recovery after acute contraction.** (A and B) siRNA-transfected HUVECs were pretreated with TNF and stimulated with thrombin for the indicated times. Cells were lysed and pull-down assays performed to detect (active) Rac1-GTP levels. (A) Effect of RhoB siRNAs on Rac1 activation. Bottom graph shows active Rac1 normalized to total Rac1 levels. Mean + SEM from al least three different experiments measuring. *, $P \leq 0.05$. (B) Effect of RhoA siRNA on Rac1 activation. Right graphs show the mean + SEM from three different experiments measuring the absolute levels of Rac1-GTP (active) and total Rac1. ***, $P = 8.85 \times 10^{-6}$. (C and D) Rac inhibition impairs barrier recovery in RhoB-transfected cells. siRNA transfected, TNF-pretreated HUVECs were stimulated with thrombin. 20 min after stimulation, 100 µM Rac inhibitor NSC23766 was added when indicated. (C) Cells were fixed and stained for the indicated proteins 72 min after stimulation. Automated image analysis was applied to detect empty areas in the cell monolayer (mask). Bar, 20 µm. (D) Analysis of TEER at 30 and 72 min after stimulation. Graph shows the mean + SEM of five different experiments. *, $P \leq 0.036$.

stimulated this Rac translocation (Palamidessi et al., 2008). Interestingly, we and others have found that HGF accelerates endothelial barrier recovery (Birukova et al., 2007, 2008), which, as we show here, is associated with increased Rac1 localization at the plasma membrane. These data indicate that Rac1 trafficking in the endothelium after thrombin-mediated acute contraction is comparable to Rac1 translocation in migrating cells and is regulated by endosomal RhoB. RhoB also regulates Rac1 negatively in cancer cell invasion (Bousquet et al., 2009) and positively in platelet-derived growth factor stimulation (Huang et al., 2011). RhoB has been proposed to link endosomal vesicles to actin filaments through its effector formins mDia1 and mDia2 (Sandilands et al., 2004; Fernandez-Borja et al., 2005; Wallar et al., 2007). Constitutively active RhoB or mDia mutants reduce the velocity of intracellular vesicles, probably by increasing the association of endosomal carriers with actin filaments (Fernandez-Borja et al., 2005; Wallar et al., 2007). We have found that RhoB depletion increases Rac1 at cell borders and reduces the trafficking of remaining Rac1 vesicles, suggesting that RhoB controls Rac1 vesicular movement toward the cell border and, hence, toward nascent cell–cell junctions. Active RhoB also accumulates with Rac1 in a Rab7-positive endosomal compartment, which suggests that RhoB activity may not only control vesicular dynamics but also divert recycling Rac1 to a late-endosomal compartment, thereby delaying the return to the plasma membrane (Fig. 9 G).

In an inflammatory context, Rac1 promotes extension of ventral lamellipodia to repair microwounds caused by adhered leukocytes undergoing diapedesis (Martinelli et al., 2013). However, the role of vesicular trafficking and Rac1 recycling has not yet been addressed for this type of membrane extension. The parallels between the signaling machinery mediating membrane extension during migration and barrier formation can be also found upstream of Rac1. Platelet-derived growth factor or HGF induces Rac1 translocation to endosomes where this GTPase encounters the GTP exchange factor Tiam1 during recycling to form actin-based migratory protrusions. In the endothelium, Tiam1 contributes to Rac1 activation in response to various barrier-stabilizing mediators (Schlegel and Waschke, 2014). Indeed, a close connection between lamellipodia and maturation of cell–cell junctions has recently been described (Abu Taha et al., 2014).

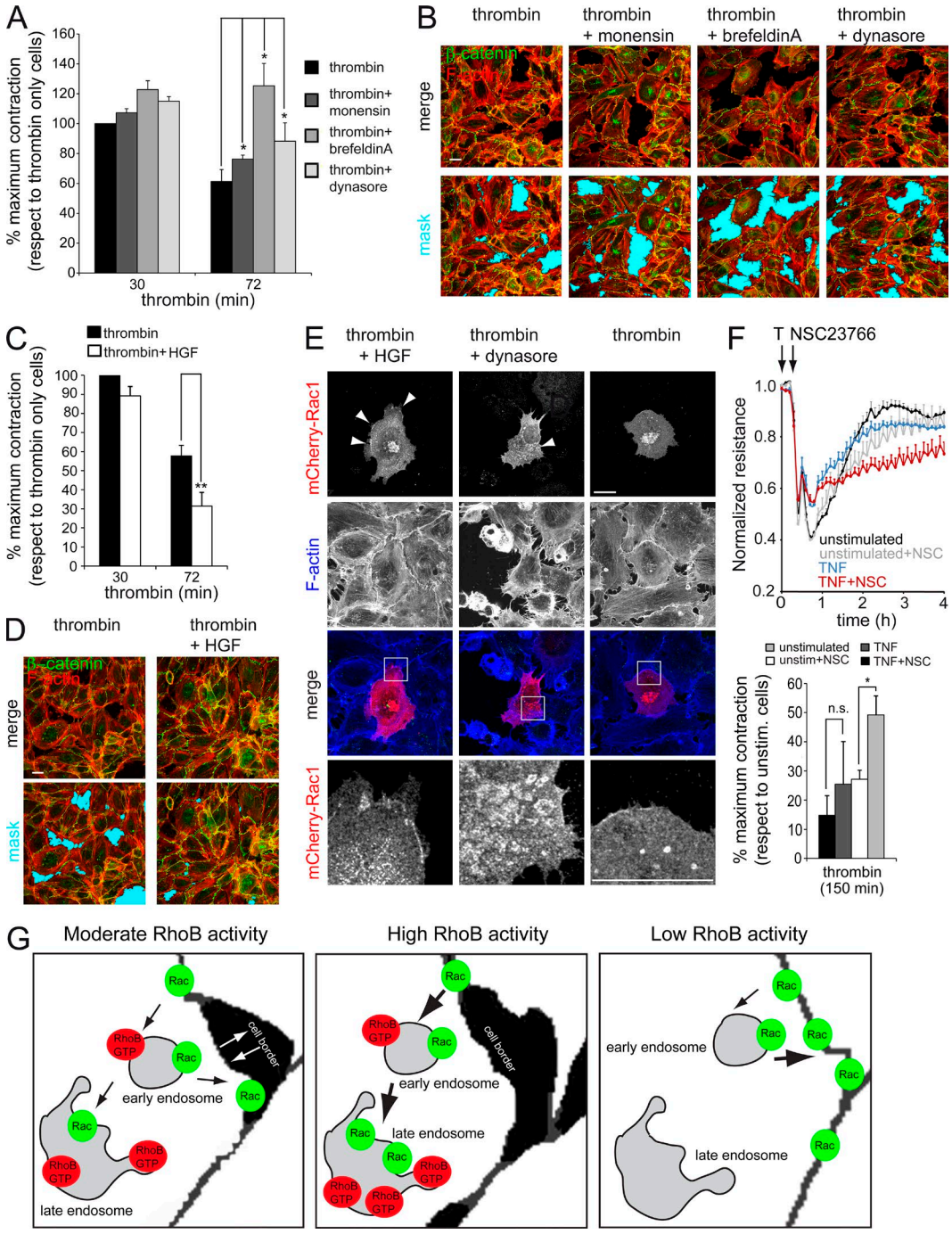

Figure 9. **Rac trafficking is essential for endothelial barrier recovery after thrombin stimulation.** (A) Inhibitors of intracellular trafficking delay barrier recovery. TNF-pretreated HUVECs were stimulated with thrombin to induce acute contraction, and after 20 min, 10 µM/l monensin and 10 µg/ml brefeldin A or 60 µM/l of the dynamin inhibitor dynasore was added when indicated. Changes in TEER were recorded and quantified at the indicated times. Graph shows the mean + SEM from four independent experiments. *, $P < 0.031$. (B) TNF-pretreated HUVECs stimulated with thrombin for 72 min in the presence or absence of the indicated inhibitors and stained for β–catenin and F-actin. Automated image analysis was applied to detect empty areas (mask). Bar, 20 µm. (C) HGF accelerates endothelial barrier reformation in TNF-pretreated endothelial cells. Relative contraction levels after thrombin stimulation at the indicated times in the presence or absence of 30 ng/ml HGF added 20 min after stimulation. Graph shows the mean + SEM of eight different experiments. **, $P = 0.006$. (D) Cells were treated as in C, fixed 72 min after thrombin stimulation, and stained for the indicated proteins. Automated image analysis was applied to detect empty areas in the cell monolayer (mask). Bar, 20 µm. (E) Effect of dynasore and HGF on mCherry-Rac1 localization. EA.hy.926 cells were transfected with mCherry-Rac1, pretreated with TNF, and stimulated with thrombin alone or in combination with dynasore and HGF as in B and D, respectively. Cells were fixed and stained for F-actin. Bar, 20 µm. (F) TNF increases endothelial sensitivity to Rac inhibition during endothelial barrier reformation. HUVECs were treated with or without TNF, and the effect of NSC23766 on endothelial barrier recovery upon acute contraction was measured by electric cell substrate impedance sensing; T, thrombin. The mean + SEM from three independent experiments is shown. *, $P = 0.011$. (G) A model for the endocytic control of Rac1 translocation to the plasma membrane through RhoB during barrier restoration. Rac1 shuttles between early endosomal compartment and the plasma membrane but is also delivered to a RhoB-positive late endosomal compartment. High RhoB levels displace Rac1 to endosomes and prevent Rac1 recycling during barrier recovery. Low RhoB activity favors Rac1 recycling to the cell border, accelerating barrier recovery after contraction.

The effect of Rac inhibition on barrier reformation between TNF-treated and resting endothelial cells is markedly different. Other researchers have reported that TNF causes a striking delay in endothelial barrier formation after thrombin-induced contraction (Paria et al., 2004). We propose that endothelial barrier disruption in response to long-term exposure to inflammatory cytokines such as TNF involves not only an increase in permeability to cells and small molecules but also a decrease in the "robustness" of the endothelial monolayer by reducing the ability of endothelial cells to reform the monolayer upon disruption. This would make the endothelium more prone to disruption by injury or edemagenic and coagulatory challenges that arise in different inflammatory contexts, particularly in chronic diseases such as Crohn's or hepatitis. Targeting negative regulators of barrier formation expressed in such contexts such as RhoB may help preserve endothelial and vascular integrity in inflammatory pathologies.

Materials and methods

Materials

Mouse monoclonal anti–VE-cadherin (catalog number 610252), mouse anti-Paxillin (catalog number 610051), and mouse anti-Rac1 (catalog number 610650) were purchased from BD. Rabbit anti–ICAM-1 (Sc-7891), rabbit anti-MLC (sc-15370), rabbit anti–ERK-1/2 (sc-94), mouse anti-RhoA (sc-418), and rabbit anti-RhoB (sc-180) for Western blot, mouse anti-RhoB (sc-8048) for immunofluorescence, and rabbit anti-RhoA/C (sc-179) were purchased from Santa Cruz Biotechnology, Inc. Rabbit anti-RhoC (D40E4) antibody was obtained from Cell Signaling Technology. Rabbit anti–β-catenin (C-2206) antibody was obtained from Sigma-Aldrich. Rabbit anti–p(T18/S19)MLC (44-260G) and anti–p(Y31) paxillin (44-720G) were obtained from Invitrogen. Goat anti–VCAM-1 (BBA19) was purchased from R&D Systems. Rat anti-HA (11867423001, clone 3F10), mouse anti-c-myc (11667149001, clone 9E10), and mouse anti-GFP (11814460001) were obtained from Roche. Phalloidin-TRITC (P-1951) was obtained from Sigma-Aldrich. Anti-IgG mouse ATTO-647N was obtained from Sigma-Aldrich (50185). Alexa Fluor 647 Phalloidin (A-22287) and To-Pro-3(T-3605) were obtained from Invitrogen. Rac1 inhibitor NSC23766 (553502), dynamin inhibitor I (dynasore; CAS 304448–55-3), and monensin (475895) were purchased from EMD Millipore. Brefeldin A (20350–15-6) was purchased from Sigma-Aldrich. Human HGF (PHG0254) was purchased from Gibco. Thrombin from human plasma (T6884) was purchased from Sigma-Aldrich. Recombinant human TNF and IL-1β was obtained from R&D Systems.

Plasmids, siRNA, and RT-qPCR analysis

Plasmid coding for HA-RhoB was from the UMR cDNA resource center (University Missouri-Rolla). Plasmids coding for HA-RhoB-V14 and GFP-RhoB were a gift from D. Pérez-Sala (Centro de Investigaciones Biolgicas, Madrid, Spain)(Centro de Investigaciones Biológicas, Madrid, Spain). To obtain a plasmid to express BirA-RhoB, a two-step procedure was followed. The sequence coding for GFP in the pEGFP-C1 expression vector was substituted by the BirA sequence. Then, the RhoB sequence was amplified by PCR and cloned between BglII and BamH1 restriction sites in the multicloning site. Plasmid coding for mCherry-Rac1 was a gift from F. Martín-Belmonte (Centro de Biología Molecular Severo Ochoa, Madrid, Spain). Plasmid from GFP-Rac1 was obtained from G. Bokoch (Scripps Research Institute, La Jolla, CA) through Addgene. Plasmid coding for GFP-Rab4 was from Gia Voeltz through Addgene. Plasmid coding for GFP-Rab5 was a gift from R. Puertollano (National Institutes of Health, Bethesda, MD). Plasmids coding for GFP-Rab7 and GFP-Rab11 were a gift of M.A. Alonso (Centro de Biología Molecular Severo Ochoa, Madrid, Spain). Plasmids coding for GFP(emerald)-Rab7 and GFP(emerald)-Rab5 were also used and were obtained from M. Davidson (Florida State University, Tallahassee, FL) through Addgene. The following siRNA oligonuceotides were obtained from the predesigned siGenome collection of Dharmacon (Vega et al., 2011): siControl1: nontargeting control, D-001210-01, 5′-UAGCGACUAAACACA ICAA-3′; siControl2: nontargeting control, D-001810-03, 5′-AUG UAUUGGCCUGUAUUAG-3′; siRhoA1: D-003860-01, 5′-AUG GAAAGCAGGUAGAGUU-3′; siRhoA2: D-003860-02, 5′-GAA CUAUGUGGCAGAUAUC-3′; siRhoB1: D-008395-07, 5′-GCA UCCAAGCCUACGACUA-3′; siRhoB2: D-008395-09, 5′-CAUCCA AGCCUACGACUAC-3′, or D-008395-08, 5′-ACACCGACGUCA UUCUCAU-3′; siRhoC1: D008555-02, 5′-AUAAGAAGGACCUGA GGCA-3′; siRhoC2: D008555-03. ON-TARGETplus SMART pool siRNA, consisting of a pool of four siRNAs, was also from Dharmacon and consisted in the following sequences: siControlpool D-001810-10, 5′-UGGUUUACAUGUCGACUAA-3′, 5′-UGGUUUACAUGU UGUGUGA-3′, 5′-UGGUUUACAUGUUUUCUGA-3′, and 5′-UGG UUUACAUGUUUUCCUA-3′; SiRhoBpool L-008395: J008395-11, 5′-GCAUCCAAGCCUACGACUA-3′; J008395-12, 5′-CAGAAC GGCUGCAUCAACU-3′; J008395-13, 5′-CGACGAGCAUGUCCG CACA-3′; and J008395-14, 5′-AAGCACUUCUGUCCCAAUG-3′. siRNA oligonucleotides were transfected with oligofectamine (Invitrogen; Fernández-Martín et al., 2012). Oligonucleotides for qPCR were from Sigma-Aldrich. One microgram of RNA from HUVECs was subjected to reverse transcription with the High Capacity RNA-cDNA kit (Applied Biosystems). RT-qPCR was performed from the resulting cDNA in a thermocycler CFX 384 (Bio-Rad) using the SsoFast EvaGreen Supermix (Bio-Rad) and the forward and reverse primers, previously designed with Probefinder software (Roche), described in Table S2 and previously used in T cells (Bhavsar et al., 2013). Parallel qPCR for the reference genes β-actin and GADPH was performed to normalize data from each point of stimulation. Triplicates from all the samples were run in parallel with non–reverse transcription controls for all the targets that yielded no detectable amplification. Unless indicated otherwise, the quantification cycle (Cq) values were in the 20–24 range, which indicates medium to high levels of these transcripts. Melting curves showed specific amplification in all cases except for RhoH. RhoH can be amplified with the same pair of oligonucleotides in T cell lines (Bhavsar et al., 2013). Relative quantification was performed with the software GenEx taking into account for corrections the efficiency of each pair of primers, the technical triplicates, and the contamination with genomic DNA, which was negligible. The relative quantification ($2^{-\Delta Cq}$) was made with respect to the expression at time 0 of TNF stimulation. Subsequently, these values were normalized again with respect a mean of the values of the reference genes. To do this, the stability of the candidate reference genes was evaluated with geNorm and Normfinder algorithms within Genex, and a combination of the two most stable was chosen to normalize the results.

Cell culture and transfection

HeLa and HepG2 cells were obtained from the American Type Culture Collection. These cells, EA.hy.926 cells and HBMEC cells were grown in DMEM supplemented with 10% FBS in an atmosphere of 5% CO_2/95% air. EA.hy.926 cells were a gift from C.J.S. Edgell (University of North Carolina, Chapel Hill, NC), and HBMECs were a gift from B. Weksler (Cornell University, Ithaca, NY). Adult HDMVECs and the CADMEC growth medium were from Tebu-Bio. HUVECs were from Lonza. For siRNA transfection, HUVECs and HDMVECs

were plated at subconfluence (10^5 cells on each well of a six-well dish) in EBM-2 medium (Lonza) with no antibiotics. The next day, cells were transfected by mixing 4 µl of oligofectamine (Invitrogen) with siRNA to a final concentration of 100 nM. At 24 h after transfection, cells were trypsinized and plated at confluence onto different dishes for parallel assays, such as permeability, adhesion, immunofluorescence or Western blotting (Aranda et al., 2013). Assays were performed 72 h after transfection. T-lymphoblasts were prepared from isolated human peripheral blood mononuclear cells. Nonadherent peripheral blood mononuclear cells were stimulated with 0.5% phytohemagglutinin for 48 h and maintained in culture medium supplemented with interleukin-2 as previously described (Reglero-Real et al., 2014). T lymphoblasts were used in experiments after culturing for 7–12 d.

Pull-down assays to detect Rho activity

HUVECs were transfected with the indicated siRNAs. After 72 h, cells were lysed and subjected to pull-down assays to analyze active, GTP-loaded RhoGTPases as previously described (Cernuda-Morollón et al., 2010; Fernández-Martín et al., 2012). In brief, cell lysates were incubated at 4°C in assay buffer with 10 µg GST-fusion proteins immobilized on GST-Sepharose beads. Active RhoA, RhoB, and RhoC were detected by pull-down with GST-rhotekin-RBD and active Rac1 with GST-PAK-PBD. Then, a fraction of the initial postnuclear supernatants and the final GST pull-down samples were subjected to SDS-PAGE in 12% acrylamide gels under reducing conditions and transferred to Immobilon-P membranes (EMD Millipore). After blocking with 5% nonfat dry milk, 0.05% (vol/vol) Tween 20 in PBS, the membranes were incubated with the indicated antibodies, washed with PBS + 0.05% Tween 20, and incubated with the appropriate secondary antibodies coupled to HRP. After subsequent extensive washes, the membranes were developed using an enhanced chemiluminescence Western blotting kit (ECL; GE Healthcare).

BioID assays

The expression vectors coding for BirA-RhoB and GFP-Rac were transfected in HEK293 cells with PEI (Sigma-Aldrich) 48 h before the assays. Cells were incubated with 50 µM biotin for 24 h, lysed and subjected to pull-down assay of biotinylated proteins with Neutravidin-Agarose (Thermo Fisher Scientific) as previously described (Roux et al., 2012; Rodríguez-Fraticelli et al., 2015;). Alternatively, cells were lysed in 25 mM Tris-HCl, pH 7.4, 1% Triton X-100, 150 mM NaCl, and 2 mM EDTA buffer containing protease inhibitors for 1 h at 4°C. After preclearing the postnuclear supernatant for 1 h with isotype-specific control immunoglobulin (Sigma-Aldrich) conjugated to protein G–Sepharose (Sigma-Aldrich), GFP-Rac was immunoprecipitated with specific anti-GFP antibodies (Roche) conjugated to protein G–Sepharose for 12 h. In parallel, a control immunoprecipitation with the isotype-specific control immunoglobulin was performed. After extensive washes with the lysis buffer, immunoprecipitates were analyzed by Western blot with anti-Rac1 antibodies and by blot with streptavidin-peroxidase (Thermo Fisher Scientific).

Endothelial permeability and leukocyte transendothelial migration assays

Permeability assays were performed as previously described (Wójciak-Stothard et al., 2001; McKenzie and Ridley, 2007). HUVECs were plated at confluence onto fibronectin-coated transwells in growth medium. After 24 h they were rinsed and stimulated or not for 20 h with TNF (10 ng/ml in growth medium) added to the top chamber of the transwell. FITC-dextran (M_r 42,000; Sigma-Aldrich) was applied apically at 0.1 mg/ml and allowed to equilibrate for 60 min before a sample of the medium was removed from the lower chamber to measure fluorescence in the Fusion α-FS fluorimeter. TEER assays with an electric cell-substrate impedance sensing system (ECIS 1600R; Applied Biophysics; Tiruppathi et al., 1992) were performed as described (Fernández-Martín et al., 2012; Aranda et al., 2013). TEER decrease during contraction and the subsequent recovery was expressed as the percentage of the difference in resistance detected between wells containing endothelial cells before and after stimulation with thrombin at the time of maximum contraction (1 U/ml thrombin in HUVECs, 0.5 h stimulation) or (10 U/ml thrombin in HDMVEC, 1 h stimulation). For transendothelial migration assays, HUVECs previously transfected with the indicated siRNAs were seeded at confluence on transwells with 5-µm-diameter pores for 48 h. T-lymphoblasts were labeled with 0.5 µm 2′,7′,-*bis*-(2-carboxyethyl)-5-(and-6)-carboxyfluorescein, acetoxymethyl ester (Molecular Probes) in serum-free medium for 20 min, washed with medium containing 10% FBS, and added to the top chamber of the HUVEC-containing transwells. 50 µg/ml SDF-1α was added to the bottom chamber as chemo attractant. After 2 h of incubation at 37°C, transmigrated T-lymphoblasts were harvested from the bottom chamber and fluorescence was measured in a Fusion α-FS fluorimeter (PerkinElmer) with a 480 nm filter. P values were calculated using Student's *t* test on a minimum of three experiments with duplicates.

Confocal and time-lapse microscopy

For confocal microscopy, cells were fixed with 4% paraformaldehyde for 20 min, blocked with TBS (25 mM Tris, pH 7.4, and 150 mM NaCl) plus 10 mM Glycine for 10 min, permeabilized for 5 min with TBS containing 0.2% Triton X-100 at 4°C, blocked with TBS containing 3% BSA for 30 min and incubated at 37°C with primary antibodies then fluorophore-conjugated secondary antibodies and 1 µg/ml TRITC/FITC/Alexa Fluor 647–labeled phalloidin. Secondary antibodies fluorophores were from Thermo Fisher Scientific and conjugated to Alexa Fluor 488, 555 and 647. Confocal laser scanning microscopy was performed with an LSM510 (ZEISS) coupled to an Axiovert200M microscope, as previously described (Fernández-Martín et al., 2012). In brief, we used 40×/1.3 oil Plan-Neofluar objective for morphological studies and 63×/1.4 oil Plan-Apochromat and 100×/1.3 oil Plan-Neofluar objectives, for image acquisition of subcellular structures. Acquisition software (LSM510 4.2) was obtained from ZEISS. Quantification of β-catenin and F-actin intensity were performed in ImageJ previous background subtraction. To quantify cell area, images of subconfluent cells stained for F-actin were taken. Quantification of Rac-cherry localization was also performed in ImageJ. In brief, images of subconfluent cells transfected for Rac1-cherry and stained for F-actin were selected. Applying a threshold, a region containing the cell area was automatically created, then made 5 to 10 pixels smaller and subtracted from the original region to generate a region comprising the fluorescence intensity at cell periphery. The main pixels intensity of Rac1-cherry images included in this peripheral region was quantified and compared with fluorescence intensity from the whole cellular area. To generate the mask marking empty spaces within a cell monolayer, a threshold to identify dark spaces was created and subsequently colored and flattened to the original image.

Time-lapse microscopy was performed with an Axiovert200 (ZEISS) microscope, in an environmental chamber at 37°C. A total of 20 mM Hepes, pH 7.4, was added to the culture medium 2 h before the experiment. Images were taken with a cooled CCD camera (Orca-ER C4742-95; Hamamatsu). Camera and shutter (Lambda Instruments) were controlled by Andor Q software. Movies were processed with ImageJ software. Vesicle tracking analysis was performed with ImageJ plugin MTrack2 and Chemotaxis and migration tool software from IBIDI.

Superresolution confocal microscopy

For stochastic optical reconstruction microscopy (STORM), cells were plated in ibiTreat, 35-mm-diameter µ-dishes from IBIDI for 24 h, starved during 1 h, pretreated with TNF, and stimulated with thrombin when indicated. Immunofluorescence was performed as described for confocal microscopy, diluting antibodies with PBS and using the 647N-atto fluorophore for the secondary antibodies. Before laser scanning, cells were washed once with distilled water and then the buffer for STORM microscopy was added (10 mM Tris, pH 8.0, 2 mM NaCl, 2% glucose, 150 mM cysteamine, 60 mM glucose oxidase, and 2 mM cyclooctatetraene). Superresolution microscopy was performed on an Eclipse Ti-E Inverted (Nikon) with an Andor Ixon camera and NIS Elements AR software, using highly inclined illumination. Superresolution images were processed with the ImageJ plugin quickPALM. The analysis of particles clustering was performed using Ripley's K-function (Kiskowski et al., 2009) programmed in C++. Stimulated emission depletion (STED) superresolution microscopy was performed on a TCS SP5 II STED microscope (Leica Biosystems), with STED being used to detect fluorescence from the ATTO-647N fluorophore. Excitation was performed using a 635-nm pulsed diode laser and de-excitation by a MaiTai tunable fs laser at 750 nm. Superresolution images are presented in inverted grayscale for a clear display of features.

Immunohistochemistry

The immunohistochemical analysis of human tissues was approved by the hospital ethics committees of the Hospital Universitario Central de Asturias and the Hospital Universitario de Salamanca were performed as described (Reglero-Real et al., 2014). In addition to biopsies from the mentioned pathologies, controls corresponded to healthy donors or to unaffected tissue of livers or intestine resected from patients with carcinoma. Formalin-fixed, paraffin-embedded sections of 4-µm thickness were deparaffinized in xylene and rehydrated through a decreasing graded-ethanol solution series. After suppression of endogenous peroxidase activity (3% hydrogen peroxide, 10 min) and antigen retrieval (boiling in 10 mM citrate buffer, pH 6.0), immunostaining was performed with a mouse monoclonal antibody against human RhoB from Santa Cruz Biotechnology, Inc. (clone C-5). Isotype-specific control was performed with anti–cytokeratin-7 from Novocastra. Anti-proteoglycan NG2 (Santa Cruz Biotechnology, Inc.) and anti–smooth muscle actin (Santa Cruz Biotechnology, Inc.) were used to identify postcapillary venules. Staining was done by using the Envision Plus peroxidase mouse system (Dako). The stained protein was visualized using DAB solution (Dako) and lightly counterstained with Mayers-hematoxylin. To ascertain the specificity of the antibody immunoreactivity, a negative control was performed in the absence of the primary antibody. In this case, no immunolabeling was detected. Immunohistochemistry was also performed on a fully automated system (Bond III; Leica Biosystems).

Online supplemental material

Fig. S1 shows changes in RhoA, RhoB, and RhoC expression in HDMECs and various cell lines. The screening of expression changes in response to TNF for the rest of the Rho GTPase family members. Fig. S2 shows the specific localization of RhoB expression in intestine fissures in intestines with Crohn's disease and controls of the immunohistochemical analysis. Fig. S3 shows a full analysis of the compensatory effects of silencing individual or pairs of RhoA subfamily GTPases. Fig. S4 shows the effect of siRhoA, siRhoB, and siRhoC on F-actin levels, adherens junction morphology, and lymphocyte transendothelial migration in TNF-stimulated HUVECs. Fig. S5 shows the lack of colocalization between endogenous RhoB and GFP-Rab4, GFP-Rab11, and endogenous EHD-1 in HUVECs and the colocalization of endogenous RhoB with cherry-Rac1 in HDMVECs. It also shows the biotynilation of Rac-GFP by RhoB-BirA in pull-down assays with neutravidin. It also shows the effect of brefeldin A on the movement of Rac1-Cherry–positive vesicles. Table S1 summarizes the RhoB expression levels detected in various human tissues. Table S2 shows the primers for qPCR analyses. Videos 1 and 2 show the effect of thrombin on GFP-RhoB intracellular trafficking in TNF-pretreated HUVECs. Videos 3 and 4 show the effect of thrombin on cherry-Rac1 intracellular trafficking in TNF-pretreated HUVECs. Videos 5 and 6 show the effect of brefeldin A on cherry-Rac1 trafficking in TNF-pretreated, thrombin-stimulated HUVECs. Online supplemental material is available at http://www.jcb.org/cgi/content/full/jcb.201504038/DC1. Additional data are available in the JCB DataViewer at http://dx.doi.org/10.1083/jcb.201504038.dv.

Acknowledgments

The expert technical advice of the Confocal Microscopy Facility, the Genomic Facility, and Dr. J. Satrústegui and L. Contreras at the Centro de Biología Molecular Severo Ochoa, Madrid, are gratefully acknowledged. The Biobank from Hospital Universitario Central de Asturias, Oviedo, is also acknowledged.

This work supported by Ministerio de Economía y Competitividad grants SAF2014-57950-R (to J. Millán), BFU2015–67266-R (to M.A. Alonso), and BFU2011-22859 (to I. Correas); Comunidad Madrid grant S2010/BMD-2305; and Cancer Research UK (A.J. Ridley). M.C. Ortega and S. Barroso are supported by Endocornea, convenio colaboración Consejo Superior de Investigaciones Científicas, from Instituto Investigaciones Sanitarias Fundación Jiménez Díaz. B. Marcos-Ramiro and D. García-Weber are recipients of a Foreign Policy Initiative fellowship from Ministerio de Economía y Competitividad.

The authors declare no competing financial interests.

Submitted: 8 April 2015
Accepted: 13 April 2016

References

Abu Taha, A., M. Taha, J. Seebach, and H.J. Schnittler. 2014. ARP2/3-mediated junction-associated lamellipodia control VE-cadherin-based cell junction dynamics and maintain monolayer integrity. *Mol. Biol. Cell.* 25:245–256. http://dx.doi.org/10.1091/mbc.E13-07-0404

Aranda, J.F., N. Reglero-Real, B. Marcos-Ramiro, A. Ruiz-Sáenz, L. Fernández-Martín, M. Bernabé-Rubio, L. Kremer, A.J. Ridley, I. Correas, M.A. Alonso, and J. Millán. 2013. MYADM controls endothelial barrier function through ERM-dependent regulation of ICAM-1 expression. *Mol. Biol. Cell.* 24:483–494. http://dx.doi.org/10.1091/mbc.E11-11-0914

Beckers, C.M., V.W. van Hinsbergh, and G.P. van Nieuw Amerongen. 2010. Driving Rho GTPase activity in endothelial cells regulates barrier integrity. *Thromb. Haemost.* 103:40–55. http://dx.doi.org/10.1160/TH09-06-0403

Bhavsar, P.J., E. Infante, A. Khwaja, and A.J. Ridley. 2013. Analysis of Rho GTPase expression in T-ALL identifies RhoU as a target for Notch involved in T-ALL cell migration. *Oncogene.* 32:198–208. http://dx.doi.org/10.1038/onc.2012.42

Birukova, A.A., E. Alekseeva, A. Mikaelyan, and K.G. Birukov. 2007. HGF attenuates thrombin-induced endothelial permeability by Tiam1-mediated activation of the Rac pathway and by Tiam1/Rac-dependent inhibition of the Rho pathway. *FASEB J.* 21:2776–2786. http://dx.doi.org/10.1096/fj.06-7660com

Birukova, A.A., N. Moldobaeva, J. Xing, and K.G. Birukov. 2008. Magnitude-dependent effects of cyclic stretch on HGF- and VEGF-induced pulmonary endothelial remodeling and barrier regulation. *Am. J. Physiol. Lung Cell. Mol. Physiol.* 295:L612–L623. http://dx.doi.org/10.1152/ajplung.90236.2008

Borissoff, J.I., H.M. Spronk, S. Heeneman, and H. ten Cate. 2009. Is thrombin a key player in the 'coagulation-atherogenesis' maze? *Cardiovasc. Res.* 82:392–403. http://dx.doi.org/10.1093/cvr/cvp066

Bousquet, E., J. Mazières, M. Privat, V. Rizzati, A. Casanova, A. Ledoux, E. Mery, B. Couderc, G. Favre, and A. Pradines. 2009. Loss of RhoB expression promotes migration and invasion of human bronchial cells via activation of AKT1. *Cancer Res.* 69:6092–6099. http://dx.doi.org/10.1158/0008-5472.CAN-08-4147

Bradley, J.R. 2008. TNF-mediated inflammatory disease. *J. Pathol.* 214:149–160. http://dx.doi.org/10.1002/path.2287

Cain, R.J., B. Vanhaesebroeck, and A.J. Ridley. 2010. The PI3K p110alpha isoform regulates endothelial adherens junctions via Pyk2 and Rac1. *J. Cell Biol.* 188:863–876. http://dx.doi.org/10.1083/jcb.200907135

Cernuda-Morollón, E., J. Millán, M. Shipman, F.M. Marelli-Berg, and A.J. Ridley. 2010. Rac activation by the T-cell receptor inhibits T cell migration. *PLoS One.* 5:e12393. http://dx.doi.org/10.1371/journal.pone.0012393

Chapman, R.E., and S. Munro. 1994. Retrieval of TGN proteins from the cell surface requires endosomal acidification. *EMBO J.* 13:2305–2312.

Compston, A., and A. Coles. 2008. Multiple sclerosis. *Lancet.* 372:1502–1517. http://dx.doi.org/10.1016/S0140-6736(08)61620-7

Croce, K., and P. Libby. 2007. Intertwining of thrombosis and inflammation in atherosclerosis. *Curr. Opin. Hematol.* 14:55–61. http://dx.doi.org/10.1097/00062752-200701000-00011

Daneshjou, N., N. Sieracki, G.P. van Nieuw Amerongen, M.A. Schwartz, Y.A. Komarova, A.B. Malik, and D.E. Conway. 2015. Rac1 functions as a reversible tension modulator to stabilize VE-cadherin trans-interaction. *J. Cell Biol.* 208:23–32. (published erratum appears in *J. Cell Biol.* 2015. 209:181) http://dx.doi.org/10.1083/jcb.201409108

Feig, L.A. 1999. Tools of the trade: use of dominant-inhibitory mutants of Ras-family GTPases. *Nat. Cell Biol.* 1:E25–E27. http://dx.doi.org/10.1038/10018

Fernandez-Borja, M., L. Janssen, D. Verwoerd, P. Hordijk, and J. Neefjes. 2005. RhoB regulates endosome transport by promoting actin assembly on endosomal membranes through Dia1. *J. Cell Sci.* 118:2661–2670. http://dx.doi.org/10.1242/jcs.02384

Fernández-Martín, L., B. Marcos-Ramiro, C.L. Bigarella, M. Graupera, R.J. Cain, N. Reglero-Real, A. Jiménez, E. Cernuda-Morollón, I. Correas, S. Cox, et al. 2012. Crosstalk between reticular adherens junctions and platelet endothelial cell adhesion molecule-1 regulates endothelial barrier function. *Arterioscler. Thromb. Vasc. Biol.* 32:e90–e102. http://dx.doi.org/10.1161/ATVBAHA.112.252080

Garcia, J.G., F. Liu, A.D. Verin, A. Birukova, M.A. Dechert, W.T. Gerthoffer, J.R. Bamberg, and D. English. 2001. Sphingosine 1-phosphate promotes endothelial cell barrier integrity by Edg-dependent cytoskeletal rearrangement. *J. Clin. Invest.* 108:689–701. http://dx.doi.org/10.1172/JCI12450

Gerald, D., I. Adini, S. Shechter, C. Perruzzi, J. Varnau, B. Hopkins, S. Kazerounian, P. Kurschat, S. Blachon, S. Khedkar, et al. 2013. RhoB controls coordination of adult angiogenesis and lymphangiogenesis following injury by regulating VEZF1-mediated transcription. *Nat. Commun.* 4:2824. http://dx.doi.org/10.1038/ncomms3824

Goldenring, J.R. 2015. Recycling endosomes. *Curr. Opin. Cell Biol.* 35:117–122. http://dx.doi.org/10.1016/j.ceb.2015.04.018

Hoeppner, L.H., S. Sinha, Y. Wang, R. Bhattacharya, S. Dutta, X. Gong, V.M. Bedell, S. Suresh, C. Chun, R. Ramchandran, et al. 2015. RhoC maintains vascular homeostasis by regulating VEGF-induced signaling in endothelial cells. *J. Cell Sci.* 128:3556–3568. http://dx.doi.org/10.1242/jcs.167601

Huang, M., L. Satchell, J.B. Duhadaway, G.C. Prendergast, and L.D. Laury-Kleintop. 2011. RhoB links PDGF signaling to cell migration by coordinating activation and localization of Cdc42 and Rac. *J. Cell. Biochem.* 112:1572–1584. http://dx.doi.org/10.1002/jcb.23069

Huveneers, S., J. Oldenburg, E. Spanjaard, G. van der Krogt, I. Grigoriev, A. Akhmanova, H. Rehmann, and J. de Rooij. 2012. Vinculin associates with endothelial VE-cadherin junctions to control force-dependent remodeling. *J. Cell Biol.* 196:641–652. http://dx.doi.org/10.1083/jcb.201108120

Kawkitinarong, K., L. Linz-McGillem, K.G. Birukov, and J.G. Garcia. 2004. Differential regulation of human lung epithelial and endothelial barrier function by thrombin. *Am. J. Respir. Cell Mol. Biol.* 31:517–527. http://dx.doi.org/10.1165/rcmb.2003-0432OC

Khan, F., B. Galarraga, and J.J. Belch. 2010. The role of endothelial function and its assessment in rheumatoid arthritis. *Nat. Rev. Rheumatol.* 6:253–261. http://dx.doi.org/10.1038/nrrheum.2010.44

Kiskowski, M.A., J.F. Hancock, and A.K. Kenworthy. 2009. On the use of Ripley's K-function and its derivatives to analyze domain size. *Biophys. J.* 97:1095–1103. http://dx.doi.org/10.1016/j.bpj.2009.05.039

Knezevic, N., M. Tauseef, T. Thennes, and D. Mehta. 2009. The G protein betagamma subunit mediates reannealing of adherens junctions to reverse endothelial permeability increase by thrombin. *J. Exp. Med.* 206:2761–2777. http://dx.doi.org/10.1084/jem.20090652

Komarova, Y.A., D. Mehta, and A.B. Malik. 2007. Dual regulation of endothelial junctional permeability. *Sci. STKE.* 2007:re8. http://dx.doi.org/10.1126/stke.4122007re8

Kroon, J., S. Tol, S. van Amstel, J.A. Elias, and M. Fernandez-Borja. 2013. The small GTPase RhoB regulates TNFα signaling in endothelial cells. *PLoS One.* 8:e75031. http://dx.doi.org/10.1371/journal.pone.0075031

Levi, M., T. van der Poll, and H.R. Büller. 2004. Bidirectional relation between inflammation and coagulation. *Circulation.* 109:2698–2704. http://dx.doi.org/10.1161/01.CIR.0000131660.51520.9A

Libby, P. 2002. Inflammation in atherosclerosis. *Nature.* 420:868–874. http://dx.doi.org/10.1038/nature01323

Lippincott-Schwartz, J., L. Yuan, C. Tipper, M. Amherdt, L. Orci, and R.D. Klausner. 1991. Brefeldin A's effects on endosomes, lysosomes, and the TGN suggest a general mechanism for regulating organelle structure and membrane traffic. *Cell.* 67:601–616. http://dx.doi.org/10.1016/0092-8674(91)90534-6

Liu, Y., K. Pelekanakis, and M.J. Woolkalis. 2004. Thrombin and tumor necrosis factor alpha synergistically stimulate tissue factor expression in human endothelial cells: regulation through c-Fos and c-Jun. *J. Biol. Chem.* 279:36142–36147. http://dx.doi.org/10.1074/jbc.M405039200

Macia, E., M. Ehrlich, R. Massol, E. Boucrot, C. Brunner, and T. Kirchhausen. 2006. Dynasore, a cell-permeable inhibitor of dynamin. *Dev. Cell.* 10:839–850. http://dx.doi.org/10.1016/j.devcel.2006.04.002

Marcos-Ramiro, B., D. García-Weber, and J. Millán. 2014. TNF-induced endothelial barrier disruption: beyond actin and Rho. *Thromb. Haemost.* 112:1088–1102. http://dx.doi.org/10.1160/TH14-04-0299

Martinelli, R., M. Kamei, P.T. Sage, R. Massol, L. Varghese, T. Sciuto, M. Toporsian, A.M. Dvorak, T. Kirchhausen, T.A. Springer, and C.V. Carman. 2013. Release of cellular tension signals self-restorative ventral lamellipodia to heal barrier micro-wounds. *J. Cell Biol.* 201:449–465. http://dx.doi.org/10.1083/jcb.201209077

McKenzie, J.A., and A.J. Ridley. 2007. Roles of Rho/ROCK and MLCK in TNF-alpha-induced changes in endothelial morphology and permeability. *J. Cell. Physiol.* 213:221–228. http://dx.doi.org/10.1002/jcp.21114

Mikelis, C.M., M. Simaan, K. Ando, S. Fukuhara, A. Sakurai, P. Amornphimoltham, A. Masedunskas, R. Weigert, T. Chavakis, R.H. Adams, et al. 2015. RhoA and ROCK mediate histamine-induced vascular leakage and anaphylactic shock. *Nat. Commun.* 6:6725. http://dx.doi.org/10.1038/ncomms7725

Millán, J., R.J. Cain, N. Reglero-Real, C. Bigarella, B. Marcos-Ramiro, L. Fernández-Martín, I. Correas, and A.J. Ridley. 2010. Adherens junctions connect stress fibres between adjacent endothelial cells. *BMC Biol.* 8:11. http://dx.doi.org/10.1186/1741-7007-8-11

Palamidessi, A., E. Frittoli, M. Garré, M. Faretta, M. Mione, I. Testa, A. Diaspro, L. Lanzetti, G. Scita, and P.P. Di Fiore. 2008. Endocytic trafficking of Rac is required for the spatial restriction of signaling in cell migration. *Cell.* 134:135–147. http://dx.doi.org/10.1016/j.cell.2008.05.034

Paria, B.C., S.M. Vogel, G.U. Ahmmed, S. Alamgir, J. Shroff, A.B. Malik, and C. Tiruppathi. 2004. Tumor necrosis factor-alpha-induced TRPC1 expression amplifies store-operated Ca2+ influx and endothelial permeability. *Am. J. Physiol. Lung Cell. Mol. Physiol.* 287:L1303–L1313. http://dx.doi.org/10.1152/ajplung.00240.2004

Pérez-Sala, D., P. Boya, I. Ramos, M. Herrera, and K. Stamatakis. 2009. The C-terminal sequence of RhoB directs protein degradation through an endo-lysosomal pathway. *PLoS One.* 4:e8117. http://dx.doi.org/10.1371/journal.pone.0008117

Popović, M., K. Smiljanić, B. Dobutović, T. Syrovets, T. Simmet, and E.R. Isenović. 2012. Thrombin and vascular inflammation. *Mol. Cell. Biochem.* 359:301–313. http://dx.doi.org/10.1007/s11010-011-1024-x

Price, L.S., J. Leng, M.A. Schwartz, and G.M. Bokoch. 1998. Activation of Rac and Cdc42 by integrins mediates cell spreading. *Mol. Biol. Cell.* 9:1863–1871. http://dx.doi.org/10.1091/mbc.9.7.1863

Reglero-Real, N., A. Alvarez-Varela, E. Cernuda-Morollón, J. Feito, B. Marcos-Ramiro, L. Fernández-Martín, M.J. Gómez-Lechón, J. Muntané, P. Sandoval, P.L. Majano, et al. 2014. Apicobasal polarity controls lymphocyte adhesion to hepatic epithelial cells. *Cell Reports.* 8:1879–1893. http://dx.doi.org/10.1016/j.celrep.2014.08.007

Ridley, A.J. 2013. RhoA, RhoB and RhoC have different roles in cancer cell migration. *J. Microsc.* 251:242–249. http://dx.doi.org/10.1111/jmi.12025

Riento, K., and A.J. Ridley. 2003. Rocks: multifunctional kinases in cell behaviour. *Nat. Rev. Mol. Cell Biol.* 4:446–456. http://dx.doi.org/10.1038/nrm1128

Rodríguez-Fraticelli, A.E., J. Bagwell, M. Bosch-Fortea, G. Boncompain, N. Reglero-Real, M.J. García-León, G. Andrés, M.L. Toribio, M.A. Alonso, J. Millán, et al. 2015. Developmental regulation of apical endocytosis controls epithelial patterning in vertebrate tubular organs. *Nat. Cell Biol.* 17:241–250. http://dx.doi.org/10.1038/ncb3106

Roshanisefat, H., S. Bahmanyar, J. Hillert, T. Olsson, and S. Montgomery. 2014. Multiple sclerosis clinical course and cardiovascular disease risk - Swedish cohort study. *Eur. J. Neurol.* 21:1353-e88. http://dx.doi.org/10.1111/ene.12518

Roux, K.J., D.I. Kim, M. Raida, and B. Burke. 2012. A promiscuous biotin ligase fusion protein identifies proximal and interacting proteins in mammalian cells. *J. Cell Biol.* 196:801–810. http://dx.doi.org/10.1083/jcb.201112098

Saibeni, S., V. Saladino, V. Chantarangkul, F. Villa, S. Bruno, M. Vecchi, R. de Franchis, C. Sei, and A. Tripodi. 2010. Increased thrombin generation in inflammatory bowel diseases. *Thromb. Res.* 125:278–282. http://dx.doi.org/10.1016/j.thromres.2009.10.012

Sandilands, E., C. Cans, V.J. Fincham, V.G. Brunton, H. Mellor, G.C. Prendergast, J.C. Norman, G. Superti-Furga, and M.C. Frame. 2004. RhoB and actin polymerization coordinate Src activation with endosome-mediated delivery to the membrane. *Dev. Cell.* 7:855–869. http://dx.doi.org/10.1016/j.devcel.2004.09.019

Scaldaferri, F., S. Lancellotti, M. Pizzoferrato, and R. De Cristofaro. 2011. Haemostatic system in inflammatory bowel diseases: new players in gut inflammation. *World J. Gastroenterol.* 17:594–608. http://dx.doi.org/10.3748/wjg.v17.i5.594

Schlegel, N., and J. Waschke. 2014. cAMP with other signaling cues converges on Rac1 to stabilize the endothelial barrier- a signaling pathway compromised in inflammation. *Cell Tissue Res.* 355:587–596. http://dx.doi.org/10.1007/s00441-013-1755-y

Shi, J., and L. Wei. 2013. Rho kinases in cardiovascular physiology and pathophysiology: the effect of fasudil. *J. Cardiovasc. Pharmacol.* 62:341–354. http://dx.doi.org/10.1097/FJC.0b013e3182a3718f

Tiruppathi, C., A.B. Malik, P.J. Del Vecchio, C.R. Keese, and I. Giaever. 1992. Electrical method for detection of endothelial cell shape change in real time: assessment of endothelial barrier function. *Proc. Natl. Acad. Sci. USA.* 89:7919–7923. http://dx.doi.org/10.1073/pnas.89.17.7919

Tiruppathi, C., T. Naqvi, R. Sandoval, D. Mehta, and A.B. Malik. 2001. Synergistic effects of tumor necrosis factor-alpha and thrombin in increasing endothelial permeability. *Am. J. Physiol. Lung Cell. Mol. Physiol.* 281:L958–L968.

Vandenbroucke, E., D. Mehta, R. Minshall, and A.B. Malik. 2008. Regulation of endothelial junctional permeability. *Ann. N. Y. Acad. Sci.* 1123:134–145. http://dx.doi.org/10.1196/annals.1420.016

van Nieuw Amerongen, G.P., R. Draijer, M.A. Vermeer, and V.W. van Hinsbergh. 1998. Transient and prolonged increase in endothelial permeability induced by histamine and thrombin: role of protein kinases, calcium, and RhoA. *Circ. Res.* 83:1115–1123. http://dx.doi.org/10.1161/01.RES.83.11.1115

van Nieuw Amerongen, G.P., C.M. Beckers, I.D. Achekar, S. Zeeman, R.J. Musters, and V.W. van Hinsbergh. 2007. Involvement of Rho kinase in endothelial barrier maintenance. *Arterioscler. Thromb. Vasc. Biol.* 27:2332–2339. http://dx.doi.org/10.1161/ATVBAHA.107.152322

Vega, F.M., G. Fruhwirth, T. Ng, and A.J. Ridley. 2011. RhoA and RhoC have distinct roles in migration and invasion by acting through different targets. *J. Cell Biol.* 193:655–665. http://dx.doi.org/10.1083/jcb.201011038

Wallar, B.J., A.D. Deward, J.H. Resau, and A.S. Alberts. 2007. RhoB and the mammalian Diaphanous-related formin mDia2 in endosome trafficking. *Exp. Cell Res.* 313:560–571. http://dx.doi.org/10.1016/j.yexcr.2006.10.033

Wheeler, A.P., and A.J. Ridley. 2004. Why three Rho proteins? RhoA, RhoB, RhoC, and cell motility. *Exp. Cell Res.* 301:43–49. http://dx.doi.org/10.1016/j.yexcr.2004.08.012

Wherlock, M., A. Gampel, C. Futter, and H. Mellor. 2004. Farnesyltransferase inhibitors disrupt EGF receptor traffic through modulation of the RhoB GTPase. *J. Cell Sci.* 117:3221–3231. http://dx.doi.org/10.1242/jcs.01193

Wojciak-Stothard, B., and A.J. Ridley. 2002. Rho GTPases and the regulation of endothelial permeability. *Vascul. Pharmacol.* 39:187–199. http://dx.doi.org/10.1016/S1537-1891(03)00008-9

Wojciak-Stothard, B., L. Zhao, E. Oliver, O. Dubois, Y. Wu, D. Kardassis, E. Vasilaki, M. Huang, J.A. Mitchell, L.S. Harrington, et al. 2012. Role of RhoB in the regulation of pulmonary endothelial and smooth muscle cell responses to hypoxia. *Circ. Res.* 110:1423–1434. http://dx.doi.org/10.1161/CIRCRESAHA.112.264473

Wójciak-Stothard, B., S. Potempa, T. Eichholtz, and A.J. Ridley. 2001. Rho and Rac but not Cdc42 regulate endothelial cell permeability. *J. Cell Sci.* 114:1343–1355.